Universidade de Brasília – UnB
Instituto de Geociências – IG
Programa de Pós-Graduação em Geologia

MINERALIZAÇÃO DE OURO NO *GREENSTONE BELT* PILAR DE GOIÁS: APLICAÇÃO DE TÉCNICAS GEOQUÍMICAS PARA DEFINIÇÃO DE VETORES PROSPECTIVOS

Dissertação de Mestrado nº 445

Rafael Rachid Barbieri Bacha

Orientadora: Profa. Dra. Catarina L. B. Toledo
Co-orientadora: Profa. Dra. Adalene M. Silva

BRASÍLIA
2019

RAFAEL RACHID BARBIERI BACHA

MINERALIZAÇÃO DE OURO NO *GREENSTONE BELT* PILAR DE GOIÁS: APLICAÇÃO DE TÉCNICAS GEOQUÍMICAS PARA DEFINIÇÃO DE VETORES PROSPECTIVOS

Dissertação de mestrado elaborada junto ao curso de Pós-graduação em Geologia (Área de concentração em Geologia Econômica), Instituto de Geociências, Universidade de Brasília, como requisito parcial para obtenção do título de Mestre em Geologia.

Orientadora: Profa. Dra. Catarina L. B. Toledo
Co-orientadora: Profa. Dra. Adalene M. Silva

Banca examinadora:
Profa. Dra. Catarina L. B. Toledo (Presidente)
Prof. Dr. José Carlos Sícoli Seoane (Membro externo)
Prof. Dr. Claudinei Gouveia de Oliveira (Membro interno)
Prof. Dr. Nilson Francisquini Botelho (Membro suplente)

BRASÍLIA
2019

FICHA CATALOGRÁFICA

Bacha, Rafael Rachid Barbieri

Mineralização de ouro no *greenstone belt* Pilar de Goiás: aplicação de técnicas geoquímicas para definição de vetores prospectivos, 2019.

Nº de páginas: 80

Área de concentração: Prospecção e Geologia Econômica

Orientadora: Prof. Dra. Catarina L. B. Toledo

“Feliz aquele que transfere o que sabe e aprende o que ensina.”

Cora Coralina

Agradecimentos

Agradeço primeiramente à minha família que sempre me apoiou nas minhas decisões e me sustentou financeiramente para que eu pudesse estudar, sem ela nada disso seria possível. Sintam-se amados Maria, Roberto, Flávia, Bianca, Natália, Alice, Amora, Bela, Luna, Bimanco e Capitu. Um agradecimento especial, beijos e abraços à minha companheira Carla e aos meus amigos Esdras, Rodrigo e Breno, que nunca me deixaram na mão mesmo nos momentos mais complicados. Sou muito grato também a todos os colegas da UnB que por algum momento participaram deste processo.

Um muito obrigado aos amigos que fiz quando trabalhei na exploração em Pilar, C1 e Riacho dos Machados, na Yamana/Brio/Leagold, valeu Baleia, Josival, Bomba, Camila, Bruna, Leo, Marcondes, Marcio e Augusto, bem como todos os outros auxiliares, técnicos e geólogos que conheci e me ajudaram em campo e interpretações geológicas.

Este tem que ser com letra maiúscula, MUITO OBRIGADO UNIVERSIDADE DE BRASÍLIA E INSTITUTO DE GEOCIÊNCIAS, incluindo todos os técnicos e professores que representam esta instituição de altíssima qualidade, essenciais nas minhas analises e nos aprendizados em sala e em campo. Foi um enorme prazer poder fazer parte deste time, um obrigado especial à minha orientadora Profa. Dra. Catarina L. B. Toledo e co-orientadora profa. Dra. Adalene M. Silva, vocês são excelentes! Que esta instituição pública continue gratuita e de qualidade.

O presente trabalho foi realizado com apoio da Coordenação de Aperfeiçoamento de Pessoal de Nível Superior – Brasil (CAPES) – Código de Financiamento 001.

Resumo

Esta pesquisa tem como objetivo testar a hipótese de que a alta razão da mobilidade dos elementos álcalis pode ser utilizada para interpretar percolação de fluidos associados a sistemas hidrotermais auríferos hospedados em rochas metassedimentares, podendo gerar vetores geoquímicos que favoreçam a descoberta de novos depósitos de ouro. Foram analisadas 469 amostras de rochas metassedimentares e máficas de dois furos de sondagem (JOT_002 e JOT_005) executados entre as minas de ouro de Pilar e Três Buracos no *greenstone belt* Pilar de Goiás, localizado no estado de Goiás. Ambos os furos de sondagem interceptaram tanto rochas mineralizadas em ouro quanto estéreis. Os resultados mostram que a proporção elementos móveis como Cs, Rb e Ba tendem a aumentar próximo aos níveis mineralizados em ouro e a diminuir conforme se distancia dos níveis. A razão $((Cs + Rb)/Th)_{UCC}$ normalizada com crosta continental superior foi selecionada como comparativo para alteração hidrotermal para avaliar e distinguir possíveis zonas mineralizadas, onde $((Cs + Rb)/Th)_{UCC} > 3$, de zonas com ausência de mineralização aurífera, onde $((Cs + Rb)/Th)_{UCC} < 3$. Nos depósitos de Pilar e Três Buracos podem ser encontradas zonas com alta mobilidade de álcalis que são de 16 a 100 vezes maior do que o halo de alteração visual. Foram identificados dois halos principais nos furos de sondagem JOT_002 e JOT_005, e ambos estão correlacionados com teores elevados de ouro. Esta razão aumenta em direção a mineralização e valores $((Cs + Rb)/Th)_{UCC} > 3$ proporcionam vetores geoquímicos que podem levar a possíveis mineralizações de ouro.

Palavras-chave: Terreno Arqueano-Paleoproterozóico de Goiás; *greenstone belt* Pilar de Goiás; depósitos de ouro hospedado em sequencias metassedimentares; mobilidade de elementos álcalis; vetores geoquímicos.

Abstract

This research aims the hypothesis that the mobility of alkali elements may be used to interpret fluid flow associated with gold-bearing hydrothermal systems hosted in metasedimentary rocks and therefore provide geochemical vectors to discover new gold deposits. The procedures involved the analysis of 469 samples of metasedimentary and mafic rock types from two drill holes (JOT_002 and JOT_005) between two gold mines (Pilar and Três Buracos) in the Pilar de Goiás greenstone belt, central Brazil. These drill holes have intercepted mineralized and barren rock types. The results reveal that the mobile elements Cs, Rb and Ba tend to be enriched in gold-bearing rock units and depleted in barren rock units. The upper continental crust normalized ratio $((Cs + Rb)/Th)_{UCC}$ *is adopted as the alteration index to evaluate and distinguish the possible mineralized zones, with* $((Cs + Rb)/Th)_{UCC} > 3$*, and barren zones with* $((Cs + Rb)/Th)_{UCC} < 3$*. In the Pilar and Três Buracos deposits can be found zones of alkali element enrichment which are 16 to 100 greater than the visible alteration halo. There are two main haloes identified in the analyzed drill holes (JOT_002 and JOT_005), and both are correlated to higher gold grades. The ratio increase towards mineralization and the values* $((Cs + Rb)/Th)_{UCC} > 3$ *provides a geochemical vector to possible gold mineralization.*

Key words: Archean-Paleoproterozoic Terrane of Goiás; Pilar de Goiás greenstone belt; metasedimentary rocks; alkali element mobility; geochemical vector.

SUMÁRIO

ÍNDICE DE FIGURAS

CAPÍTULO I - INTRODUÇÃO

1 Apresentação

Os terrenos arqueanos e paleoproterozóicos possuem componentes importantes chamados de associações "*granite-greenstone belt*", que são terrenos alongados compostos por sequências vulcanossedimentares e suítes tonalito-trondhjemito-granodiorito (TTG) que datam do Eoarqueano (>3,6 Ga) ao final do Neoarqueano (~2,5 Ga; Tang e Santosh, 2017). Segundo Van Kranendonk (2007), nesses terrenos, são encontrados importantes informações relacionadas à tectônica de acresção, tanto lateral quanto vertical, referente à evolução crustal da Terra primitiva.

O termo "*greenstone belt*" remonta às pesquisas geológicas canadenses por volta de 1870. Embora tenham passado quase 150 anos desde sua primeira utilização, não existe uma simples definição para um *greenstone belt* (de Wit, 2004). De acordo com Furnes *et al*. (2015), os *greenstone belts* são terrenos alongados, podendo apresentar diversas formas, compostos por rochas ultramáficas, máficas a félsicas extrusivas e geralmente associados a diferentes quantidades e variabilidades de rochas sedimentares.

Os *greenstone belt* são conhecidos por hospedarem depósitos auríferos, associados a zonas de falha e cisalhamento em terrenos deformados, na maioria dos casos em fácies xisto verde superior (Dubé e Gosselin, 2007). Esses depósitos foram difundidos na comunidade científica como "*lode deposits*" (Poulsen *et al*., 2000), também conhecidos pelos termos orogênico, mesotermal, "*gold-only*", "*shear-zone-related*" e "*quartz-carbonate vein*", segundo diversos autores (Kerrich e Feng, 1992; Hodgson, 1993; Robert, 1995; Groves *et al*., 1998; Poulsen *et al*., 2000; Groves *et al*., 2003; Goldfarb *et al*., 2005). De acordo com Dubé e Gosselin (2007), são depósitos com geologia, história e evolução complexas, hospedados em terrenos metamórficos deformados e consistem de sistemas auríferos complexos, comumente com veios quartzo-carbonáticos do tipo *fault-fill* com mergulho moderado, associados a regimes compressivos rúptil-dúctil em zonas de cisalhamento e falhas, localmente conectados a veios extensivos tardios e brechas hidrotermais.

O Terreno Arqueano-Paleoproterozoico de Goiás (TAPG) é um fragmento de idade Arqueana-Paleoproterozoica, localizado na porção centro-oeste do Estado de Goiás, que pode ter sido amalgamado durante o Ciclo Brasiliano na margem oeste da Faixa Brasília (Jost *et al*., 2014). Esse terreno é composto por TTGs (tonalito-trondhjemito-granodiorito) e *greenstone belts* e possui aproximadamente 18.000 km². Os TTGs perfazem 80% da área e estão distribuídos nos Complexos Uvá, Caiçara, Anta, Caiamar, Moquém e Hidrolina, de sudoeste para nordeste. Os *greenstone belts* cobrem 20% desse Terreno e são representados pelos

greenstone belt Serra de Santa Rita, Faina, Crixás, Guarinos e Pilar de Goiás (**Figura 1**). Todos os *greenstone belt* estão metamorfizados em fácies xisto verde superior a anfibolito e hospedam importantes depósitos auríferos, conhecidos desde a época dos bandeirantes pelos garimpos até atualmente pelas diversas minas de ouro (Faina – Mina Cascavel; Guarinos – Mina Maria Lázara e Caiamar; Pilar de Goiás – Mina Pilar; Crixás – Mina III e Mina Nova).

O *greenstone belt* Pilar de Goiás está localizado na porção norte do TAPG e é subdividido em quatro formações (Jost e Oliveira, 1991). A base da sequência é constituída predominantemente por rochas metavulcânicas ultramáficas e máficas representadas pelas formações Córrego Fundo e Cedrolina, respectivamente. Essas sequências vulcânicas estão recobertas por duas sequências sedimentares distintas interpretadas por alguns autores como unidades alóctones posicionadas em escamas tectônicas (Resende e Jost, 1995). A inferior, Formação Boqueirão, com aproximadamente 250 metros de espessura, é uma sucessão de rochas calcissilicáticas com metarenitos finos calcíferos e lentes de dolomito, interpretadas como um resíduo de margem continental passiva alóctone, que repousa tectonicamente sobre os metakomatiitos da Formação Córrego Fundo, e os metabasaltos da Formação Cedrolina. A superior, Formação Serra do Moinho, com espessura aproximada de 300 metros, repousa tectonicamente sobre a Formação Boqueirão, composta por metagrauvacas, metapelitos carbonosos, xistos com variáveis proporções de quartzo, clorita, muscovita, biotita, anfibólio e grafita, e intrusões ígneas por vezes metamorfizadas. As ocorrências auríferas foram encontradas hospedadas na Formação Serra do Moinho.

A proposta desta pesquisa é estabelecer os principais controles da mineralização de ouro no *greenstone belt* Pilar de Goiás e estabelecer os vetores geoquímicos de exploração para a região. Pretende-se com esta pesquisa contribuir para a descoberta de futuros depósitos auríferos no *greenstone belt* Pilar de Goiás como um todo.

1.1 Objetivos da dissertação

O objetivo principal desta dissertação é caracterizar os controles da mineralização de ouro no *greenstone belt* Pilar de Goiás e identificar vetores geoquímicos com base na mobilidade de elementos álcalis.

Os objetivos específicos incluem:

i. Mapeamento geológico do depósito Três Buracos em escala 1:15.000, visando definir a sua estratigrafia e posicionar as zonas mineralizadas;
ii. Caracterização petrográfica das diferentes unidades, visando à identificação dos protólitos e dos diferentes eventos termotectônicos e hidrotermais atuantes nos depósitos Três Buracos e Pilar;
iii. Caracterização das principais zonas mineralizadas dos depósitos Três Buracos e Pilar, com definição do posicionamento estratigráfico e controle estrutural dos veios mineralizados;
iv. Identificação das assembleias minerais proximais e distais nas zonas de alteração hidrotermal adjacentes aos veios de quartzo mineralizados;
v. Estudo da mobilidade dos álcalis nas zonas de alteração hidrotermal e definição de vetores prospectivos;

1.2 Estruturação da dissertação

Esta dissertação de mestrado está organizada em três partes:

1. Breve apresentação, objetivos da dissertação e síntese da geologia do Terreno Arqueano-Paleoproterozoico de Goiás;
2. Artigo científico intitulado "**ALKALI ELEMENT MOBILITY ASSOCIATED WITH GOLD MINERALIZATION IN THE PILAR DE GOIÁS GREENSTONE BELT, CENTRAL BRAZIL**";
3. Considerações finais e sugestões para trabalhos futuros.

1.3 Síntese da geologia do Terreno Arqueano-Paleoproterozoico de Goiás

1.3.1 Contexto geológico

A Província Tocantins (Almeida *et al.*, 1981) de idade Neoproterozoica é considerada como um sistema orogênico que está entre os crátons São Francisco e Amazônico. Acredita-se que o seu desenvolvimento foi devido aos eventos colisionais responsáveis pela agregação do supercontinente Gondwana ao final do Neoproterozoico. Inserida na Província Tocantins, a Faixa Brasília bordeja o Cráton do São Francisco (CSF), enquanto as faixas Araguaia e Paraguai bordejam o Cráton Amazônico (Valeriano *et al.*, 2004). É possível que ainda um

terceiro bloco tenha contribuído no desenvolvimento da Província Tocantins, o Cráton do Paraná ou Paranapanema, que está encoberto pela Bacia do Paraná (Brito Neves *et al*., 1999). A Província Tocantins foi dividida, segundo Fuck *et al.* (1993) e Fuck (1994), de leste para o oeste: Zona Cratônica, Faixa Brasília, Maciço de Goiás, Arco Magmático de Goiás e Faixa Paraguai-Araguaia.

Com relação à compartimentação tectônica e localização das unidades que compõem a Faixa Brasília, foram definidos de leste para oeste os terrenos que agregaram à borda ocidental do CSF: metassedimentos parautóctones do Grupo Bambuí na zona de antepaís; metassedimentos alóctones da margem passiva neoproterozoica e rochas do seu embasamento; o Maciço Goiano, considerado um microcontinente composto por rochas arqueanas e mesoproterozoicas; e o Arco Magmático de Goiás, responsável pelo magmatismo pré-colisional desde ca. 880 Ma até ca. 640 Ma, momento em que foi acrescida a faixa orogênica (Valeriano *et al*., 2004).

A Faixa Brasília é composta por unidades de rochas supracrustais depositadas e deformadas sobre a borda oeste do CSF, sendo o metamorfismo e a deformação gradualmente mais ativos para o oeste (Pimentel *et al*., 2004). A Faixa Brasília **(Figura 1)** é delimitada em duas porções distintas, a Faixa Brasília Meridional (FBM), com orientação NW, e a Faixa Brasília Setentrional (FBS), com orientação NE. No contato entre esses dois ramos, formou-se a Megaflexura dos Pireneus, que acentuou na Faixa Brasília uma concavidade voltada para leste, corroborando com uma proeminência do contorno original da margem do paleocontinente São Francisco (Valeriano *et al*., 2004). De acordo com Jost *et al*. (2014), cada ramo apresenta evolução geológica e metalogenética própria, e dados geocronológicos propõem que a evolução da região foi policíclica com eventos desde o Arqueano até o Paleoproterozoico, ainda com reciclagem parcial no Neoproterozoico.

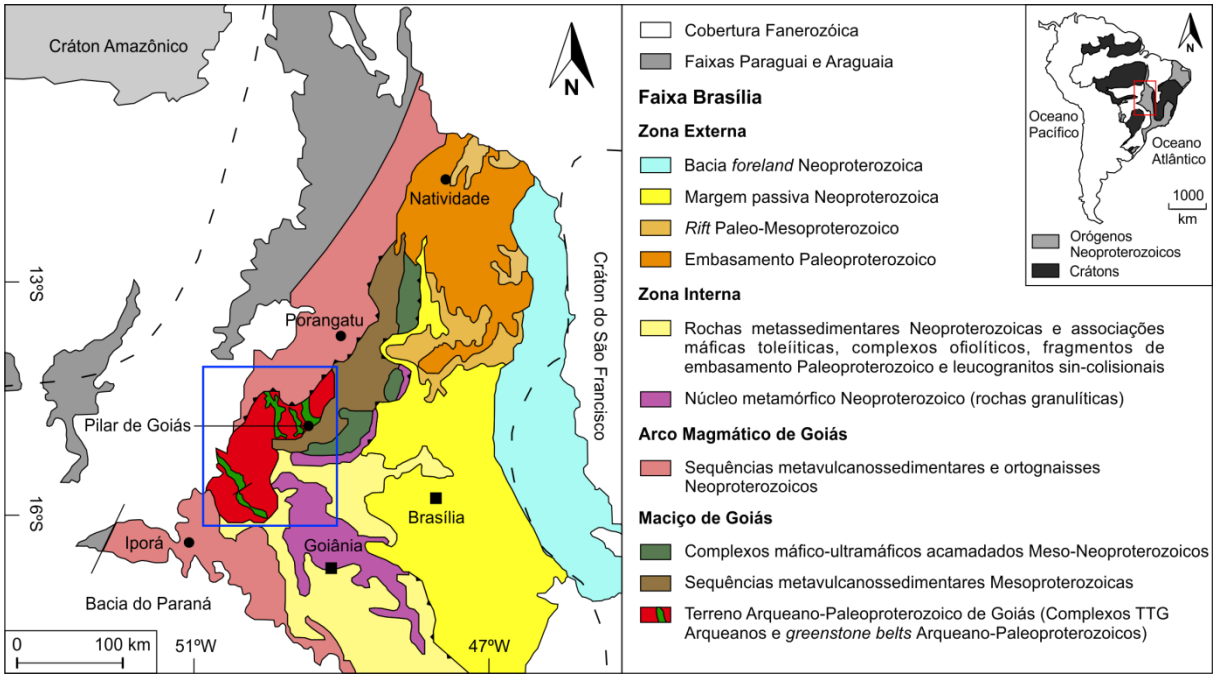

Figura 1. Mapa geológico simplificado da Faixa Brasília com localização do Terreno Arqueano-Paleoproterozoico de Goiás (Adaptado de Pimentel *et al.* 2004). O quadrado azul indica a posição da Figura 2.

As porções norte e sul ainda são divididas em zonas interna e externa. A zona interna é composta por três unidades distintas: (1) Complexo Granulítico Anápolis-Itauçu (Piuzana *et al.*, 2003) e Complexo Uruaçu (Giustina *et al.*, 2009), que fazem parte de um núcleo metamórfico de um orógeno; Grupo Araxá (Seer *et al.*, 2001), representado por rochas metassedimentares; e fragmentos ofiolíticos (Strieder e Nilson, 1992); (2) Terreno Arqueano-Paleoproterozoico de Goiás (ou Maciço de Goiás), composto por fragmentos cratônicos alóctones (Jost *et al.*, 2014); complexos máfico-ultramáficos acamadados com sequências vulcanossedimentares (Ferreira Filho *et al.*, 1992; Ferreira Filho *et al.*, 1994; Moraes e Fuck, 2000); e (3) Arco Magmáfico de Goiás, composto por sequências metavulcanossedimentares e ortognaisses Neoproterozoicos, que representam uma crosta continental juvenil formada durante a convergência de placas entre 900 e 630 Ma (Pimentel *et al.*, 1991, 1997; Pimentel e Fuck, 1992; Junges *et al.*, 2002, 2003). Segundo Laux *et al.* (2005), houveram dois episódios de atividade ígnea no Arco Magmático de Goiás: o primeiro, entre 890 e 800 Ma em arcos intraoceânicos; e o segundo, entre 660 e 600 Ma em ambiente de margem continental ativa no final do Ciclo Brasiliano.

1.3.2 Os complexos TTG

O TAPG é representado em cerca de 80% por terrenos TTG, estes compostos por ortognaisses tonalíticos a granodioríticos, divididos em seis complexos cada um, com sua peculiaridade em termos estruturais, litológicos e idade. Os complexos são divididos pela localização geográfica: ao sul, estão os complexos Uvá e Caiçara; e, ao norte, estão os complexos Hidrolina, Moquém, Caiamar e Anta.

Dentre os complexos TTG do sul, o complexo Caiçara é composto em maior predominância por ortognaisses tonalíticos com idade de cristalização U-Pb em zircão 3,14 Ga e idade-modelo Sm-Nd mínima de 3,1 Ga, estes que são intrudidos por corpos de granodiorito, granito e rochas da série charnockítica, com idade de cristalização U-Pb em zircão 2,8 Ga e idade-modelo Sm-Nd de 2,9 Ga (Beghelli Junior, 2012). O segundo complexo do sul, Uvá, é constituído por dois grupos de ortognaisses e localiza-se no extremo sul do TAPG (Jost *et al*., 2005). O grupo mais predominante é o mais antigo, que é caracterizado por ortognaisses polideformados tonalíticos a granodioríticos, e *stocks* de diorito. Os ortognaisses tonalíticos foram datados pelo método U-Pb em zircão e apresentaram idade entre 3,040 a 2,93 Ga (Jost *et al*., 2013), enquanto o *stock* de diorito, datado pelo mesmo método, apresentou idade de 2,934 Ga (Pimentel *et al*., 2003). O grupo menos predominante é composto por corpos tabulares de tonalito e monzogranito, que, segundo Jost *et al*. (2005, 2013) apresentaram idades de cristalização U-Pb em zircão entre 2,764 e 2,846 Ga.

Os complexos TTG da região norte, Anta, Caiamar, Moquém e Hidrolina estão divididos em dois estágios de granitogênese. O primeiro estágio, presente nos complexos Anta, Hidrolina e Caiamar, fora responsável pela geração de ortognaisses tonalíticos a granodioríticos, e, em menor proporção, graníticos. A idade de cristalização U-Pb em zircão desse estágio varia entre 2,845 e 2,785 Ga. Segundo Queiroz *et al*. (2008), idades-modelo Sm-Nd de 3,0 Ga e cristais herdados de zircão entre 3,15 a 3,3 Ga sugerem que magmas juvenis foram contaminados por crosta siálica mais antiga, sem evidências de exposição até o presente. O segundo estágio, preservado no complexo Moquém, é composto por corpos tabulares foliados de granodiorito e granito com idades de cristalização entre 2,711 e 2,707 Ga. Ainda, Queiroz *et al*. (2008) apontam que não foi detectada reciclagem isotópica durante o Paleoproterozoico e Neoproterozoico em dados U-Pb, provavelmente pois esses processos atuantes ocorrem em temperatura inferior à da estabilidade isotópica do sistema U-Pb-Th. Logo, os dados sugerem que o substrato arqueano da região é policíclico, e os complexos TTG da porção norte do TAPG são mais recentes que os complexos TTG da região sul.

1.3.3 Os *greenstone belts*

O TAPG é representado por *greenstone belts* em aproximadamente 20% da sua área, estes ocorrem como faixas alongadas e relativamente estreitas, individualizados em cinco *greenstone belts* distintos e localizados entre os complexos TTG **(Figura 2)**. Três deles (Crixás, Guarinos e Pilar de Goiás) se localizam na região norte, e dois (Faina e Serra de Santa Rita) na região sul do TAPG. De acordo com observações feitas por Jost *et al*. (2005, 2013), o contato dos *greenstone belts* com os complexos TTG é tectônico, e a ocorrência de *klippen* nos ortognaisses sugerem que as rochas supracrustais são alóctones. Os cinco *greenstone belts* possuem registros estratigráficos semelhantes, sendo compostos na base por komatiitos, sobrepostos por metabasaltos, seguidos por porções superiores de rochas metassedimentares. O metamorfismo também é semelhante nos cinco *greenstone belts*, estão todos em fácies xisto verde a anfibolito, o que, somado a estado fragmentário, adelgaçamento, espessamento, deformação policíclica e à quantidade limitada de horizontes-guias, dificulta a reconstrução original das faixas (Jost *et al*., 2014).

De acordo com Jost *et al*. (2014), os *greenstone belts* do TAPG possuem diversos depósitos auríferos e potenciais depósitos singenéticos de ferro em formações ferríferas bandadas, ferro e manganês do tipo SEDEX, ouro associado a albititos, VMS e paleoplacer, e níquel e cobre associados a metakomatiitos, sendo que a maioria desses potenciais depósitos carecem de estudos.

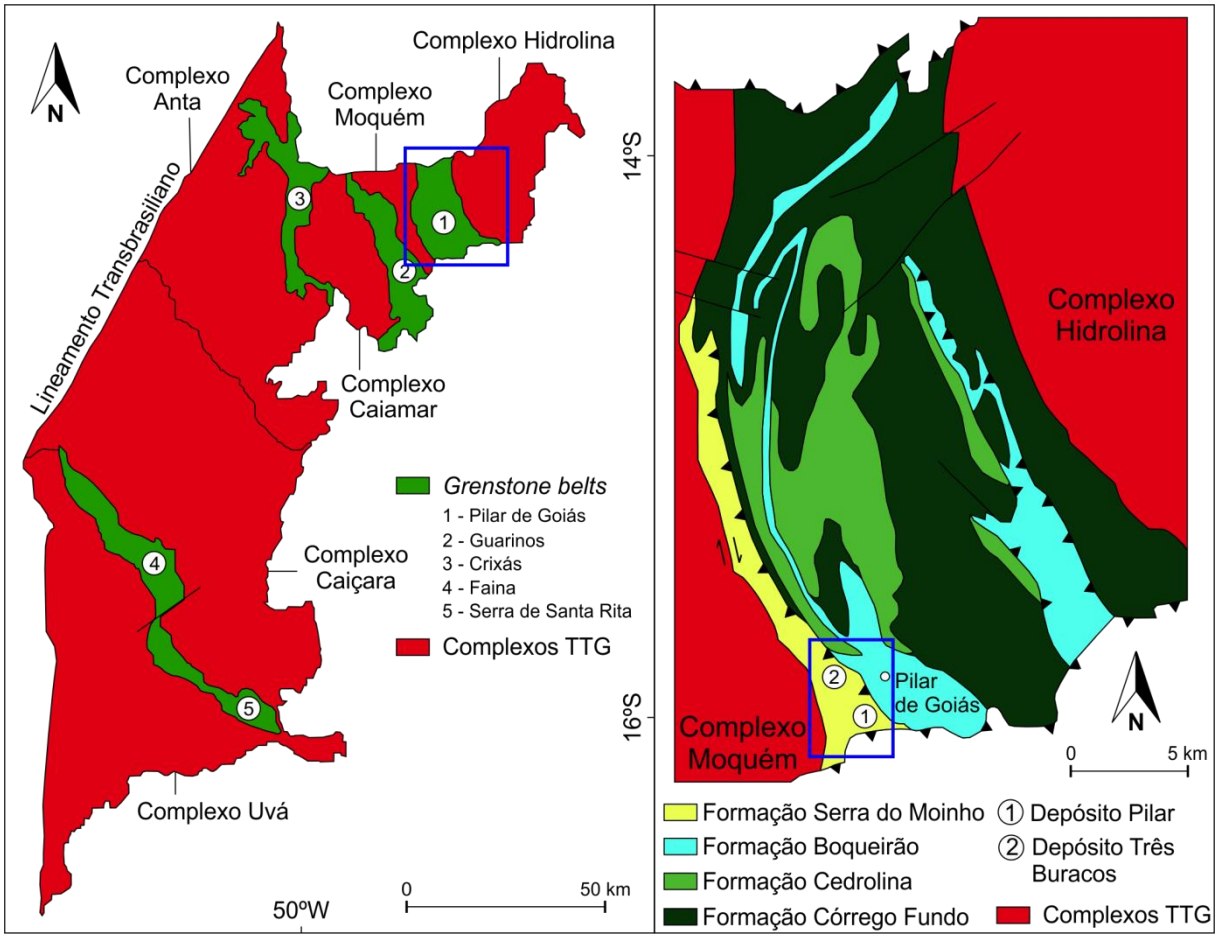

Figura 2. Localização detalhada dos cinco *greenstone belts* do Terreno Arqueano-Paleoproterozoico de Goiás e mapa geológico simplificado do *greenstone belt* Pilar de Goiás. Adaptado de Jost *et al*. (2014).

1.3.3.1 Estratigrafia

O primeiro estudo de modelo estratigráfico para os três *greenstone belts* da região norte (Crixás, Guarinos e Pilar de Goiás) do TAPG remonta a Danni e Ribeiro (1978), que agruparam as unidades metavulcanossedimentares da região norte no Grupo Pilar de Goiás, utilizando o *greenstone belt* Pilar de Goiás como seção-tipo. O Grupo Pilar de Goiás foi dividido por Sabóia (1979), da base para o topo, em formações Córrego Alagadinho, Rio Vermelho e Ribeirão das Antas, representadas por metakomatiitos, metabasaltos e rochas metassedimentares, respectivamente, utilizando a Sequência Crixás como seção-tipo. Posteriormente, os três *greenstone belts* da região norte foram considerados como unidades independentes por Jost e Oliveira (1991), devido aos contrastes litológicos, variações no vulcanismo e nos ambientes deposicionais registrados nas sequencias sedimentares. Logo, cada *greenstone belt* foi contemplado com um grupo (Crixás, Guarinos e Pilar de Goiás) e unidades formais para agrupar os conteúdos estratigráficos respectivos.

O primeiro modelo estratigráfico para os *greenstone belts* da região sul (Faina e Serra de Santa Rita) foi proposto por Danni *et al*. (1981), em que subdividiram as faixas na Sequência Serra de Santa Rita (inferior) e Sequência Serra do Cantagalo (superior). A Sequência Serra de Santa Rita é composta por rochas metavulcânicas e metassedimentares arqueanas, enquanto a Sequência Serra do Cantagalo é representada por rochas metassedimentares mais jovens em discordância com a sequência inferior. Contemporaneamente, Teixeira (1981) propôs o termo Grupo Goiás Velho, composto por uma unidade inferior representada por rochas metavulcânicas, com komatiitos, metabasaltos e metavulcânicas félsicas, e uma unidade superior metassedimentar, que inclui as rochas da Sequência Serra do Cantagalo proposta por Danni *et al*. (1981). Conforme observado por Teixeira (1981), nas rochas supracrustais das duas faixas havia diferenças significativas, logo foram subdivididas em *greenstone belt* Faina e *greenstone belt* Serra de Santa Rita, separados por uma falha transcorrente dextral. Posteriormente, foi proposto por Resende *et al*. (1998) um modelo estratigráfico independente para cada *greenstone belt* (Faina e Serra de Santa Rita), visto que, apesar de ambos possuírem sequências metavulcânicas inferiores semelhantes, as unidades metassedimentares superiores são distintas.

1.3.3.2 Sequências metavulcânicas

Os cinco *greenstone belts* do TAPG possuem a base de suas respectivas colunas estratigráficas muito semelhantes, sendo compostos por metakomatiitos sobrepostos por metabasaltos. Os nomes dados para as formações que compreendem os metakomatiitos são Córrego Fundo (*greenstone belt* Pilar de Goiás), Serra do Cotovelo (*greenstone belt* Guarinos), Córrego Alagadinho (*greenstone belt* Crixás) e Manoel Leocádio (*greenstone belts* Serra de Santa Rita e Faina). Para os metabasaltos são as seguintes formações: Cedrolina (*greenstone belt* Pilar de Goiás), Serra Azul (*greenstone belt* Guarinos), Rio Vermelho (*greenstone belt* Crixás) e Digo-Digo (*greenstone belts* Serra de Santa Rita e Faina).

Os metakomatiitos foram reportados na literatura por diversos grupos de pesquisadores (Danni *et al*., 1981; Teixeira, 1981; Teixeira *et al*., 1981; Kuyumijan e Teixeira, 1982; Danni *et al*., 1986; Jost *et al*, 1995), e feições vulcânicas originais como brechas de fluxo, *pillow lavas*, textura cumulática e *spinifex* foram encontradas nos terrenos *greenstone belt* do TAPG. De acordo com Jost *et al*. (2014), os metabasaltos são predominantemente toleíticos, raramente apresentando estrutura almofadada, e ainda contam com a presença de diques e *sill* gabróicos.

Intercalado aos metakomatiitos e metabasaltos, ocorrem metachert, gonditos e formações ferríferas; estas intercalações estão presentes em todos os *greenstone belts* do TAPG e apresentam espessuras variadas, o que sugere que cada *greenstone belt* gerou vulcanismo com características rítmicas individuais, assim como estado de preservação. Em geral, os derrames apresentam variadas proporções de plagioclásio e ferroactinolita, e, subordinadamente, titanita, clorita, clinozoisita, quartzo, pirita e magnetita (Jost *et al*., 2014).

1.3.3.3 Sequências metassedimentares

Os intervalos metassedimentares localizados nas sequências de topo dos *greenstone belts* do TAPG apresentam características distintas. Essa variação é presente tanto no tipo de contato das sequências metassedimentares com as unidades metabasálticas, quanto na diversidade de rochas e espessura das camadas metassedimentares.

De acordo com as observações de Resende e Jost (1995), as unidades metassedimentares no *greenstone belt* Pilar de Goiás ocorrem em duas escamas tectônicas. Essas escamas foram denominadas Formação Boqueirão (inferior) e Formação Serra do Moinho (superior). A Formação Boqueirão repousa tectonicamente sobre a Formação Cedrolina (metabasaltos) e é composta por intercalações de lentes de metadolomito com metarenitos calcíferos finos, e é interpretada como um resíduo de margem continental passiva alóctone. A Formação Serra do Moinho está posicionada por tectônica acima da Formação Boqueirão e é representada por metagrauvacas semelhantes às metagrauvacas dos *greenstone belts* Guarinos e Crixás, entretanto são levemente distintas no quesito espessura das camadas e textura da rocha. Jost *et al*. (2014) sugerem que o *greenstone belt* Crixás seria o mais proximal da fonte das rochas sedimentares, pois foi notado que o tamanho médio da granulometria das rochas metassedimentares cresce do *greenstone belt* Pilar de Goiás em direção ao *greenstone belt* Guarinos e, sucessivamente, ao *greenstone belt* Crixás.

No *greenstone belt* Guarinos, o pacote metassedimentar é subdividido em quatro formações, da base para o topo, Formação São Patricinho, Formação Aimbé, Formação Cabaçal e Formação Mata Preta (Jost *et al*., 2014). A Formação São Patricinho é formada por metarritmitos finos com alta proporção em clorita e presença de clastos de metabasaltos, levando à hipótese de que esses metarritmitos foram formados a partir da desagregação das rochas metavulcânicas posicionadas estratigraficamente abaixo dos metarritmitos. A Formação Aimbé e a Formação Cabaçal são descritas por Resende e Jost (1994) e Resende e Jost (1995), a Formação Aimbé é formada por zonas de alteração hidrotermal com condutos

exalativos e lentes de paraconglomerado sobrepostos por camadas de formação ferrífera bandada e metargilitos, que grada suavemente para a Formação Cabaçal, que é composta por camadas espessas de metapelitos carbonosos. Recentemente, as metagrauvacas de topo que eram classificadas como Membro Superior da Formação Cabaçal por Jost *et al*. (1995), foram reclassificadas como Formação Mata Preta (Jost *et al*., 2012).

As rochas metassedimentares do *greenstone belt* Crixás foram nomeadas como Formação Ribeirão das Antas por Jost e Oliveira (1991), e são compostas por metapelitos carbonosos de ambiente euxênico, intercalados por metadolomitos e metabasaltos. Conforme se aproxima ao topo da sequência, as grauvacas rítmicas passam a predominar, enquanto os pelitos gradualmente diminuem.

No *greenstone belt* Faina, as rochas metassedimentares foram classificadas em Formação Fazenda Tanque, Formação Serra de São José e Formação Córrego do Tatú, sendo que a primeira representa um ciclo plataformal completo, e a segunda e a terceira, outro ciclo completo (Resende *et al*., 1998). As unidades são representadas por metaconglomerados, metarenitos, metapelitos, metadolomitos e formações ferríferas bandadas, respectivamente.

A seção metassedimentar do *greenstone belt* Serra de Santa Rita foi nomeada por Resende *et al*. (1998) de Formação Fazenda Limeira, e descrita por eles como uma sequência de metapelitos carbonosos, seguidos de metachert, metadolomitos e formações ferríferas bandadas ao topo. Acredita-se que essa formação possui correlação com o segundo ciclo sedimentar do *greenstone belt* Faina.

1.3.3.4 Atividade magmática Paleoproterozoica

O substrato Arqueano do TAPG passou pelo estágio de cratonização em aproximadamente 2,7 Ga; todavia o TAPG possui influência de atividade magmática de idade Paleoproterozoica.

Segundo Corrêa da Costa (2003), os complexos Caiçara e Anta hospedam enxames de diques máficos com idades Sm-Nd de 2,3 a 2,5 Ga, provavelmente devido a uma fase de distensão crustal. No Complexo Hidrolina, foram identificadas por Danni *et al*. (1986) intrusões de diques máficos dioríticos em um lineamento transcorrente, com idade U-Pb em zircão de 2146 ± 1,6 Ma (Jost *et al*., 1992). Nos três *greenstone belts* da porção norte foram identificados *stocks* e *sills* de albita-granito em falhas de empurrão (Jost *et al*., 1992), com idades U-Pb em zircão de 2145 ± 12 Ma (Queiroz, 2000). No *greenstone belt* Crixás, diques

máficos com idade U-Pb em zircão de 2170 ± 17 Ma interceptam a mineralização aurífera (Jost *et al*., 2010).

De acordo com Jost *et al.* (2014), os dados sugerem a hipótese de que, após a cratonização, o TAPG passou por um ciclo completo de abertura no Sideriano, posteriormente por um ciclo de fechamento de orógeno no Riaciano, e que a ampla distribuição geográfica dos eventos inferem que estes ocorreram em áreas periféricas de uma faixa móvel.

1.3.3.5 Ciclo Brasiliano

Após o fechamento do orógeno no Riaciano, provavelmente o TAPG permaneceu estável ou sem registros até o Neoproterozoico.

Foram registradas intrusões de muscovita-granito no *greenstone belt* Serra de Santa Rita e nos complexos Uvá e Caiçara (Jost *et al*., 2005) com idade U-Pb em zircão de 625 ± 6 Ma (Pimentel *et al*., 2003). No extremo norte do *greenstone belt* Guarinos, pode ser encontrada uma intrusão de dique de albitito aurífero, com idade U-Pb em zircão de 729 ± 15 Ma (Rodrigues, 2011). No Complexo Moquém, são encontradas finas bandas félsicas com idade U-Pb em zircão de 590 ± 10 Ma, interpretadas por Queiroz *et al*. (2008) como anatexia parcial dos ortognaisses. Nos ortognaisses arqueanos, a hipótese de reciclagem parcial de cristais de zircão magmáticos, identificada pelos interceptos inferiores de idade U-Pb entre 750 e 590 Ma (Queiroz *et al*., 2008), e, nas rochas metassedimentares dos *greenstone belt* Pilar de Goiás, Guarinos e Crixás, reciclagem de cristais detríticos, com idades entre 500-450 Ma (Tassinari *et al*., 2006). Em depósitos auríferos no *greenstone belt* Crixás, foram encontradas paragêneses de zonas de alteração hidrotermal com idades Ar-Ar, Rb-Sr, K-Ar e Sm-Nd de 600 a 550 Ma (Fortes *et al.*, 2003).

CAPÍTULO II – *ALKALI ELEMENT MOBILITY ASSOCIATED WITH GOLD MINERALIZATION IN THE PILAR DE GOIÁS GREENSTONE BELT, CENTRAL BRAZIL*

Bacha, R.R.B., Toledo, C.L.B., Silva, A.M.

Abstract

This research aims to evaluate the mobility of alkali elements associated with gold-bearing hydrothermal systems hosted in metasedimentary rocks in the Pilar de Goiás greenstone belt, central Brazil, and provide geochemical vectors to discover new gold deposits. The procedures involved the analysis of 469 samples of metasedimentary and mafic rock types from two drill holes performed between two gold mines (Pilar and Três Buracos) in the Pilar de Goiás greenstone belt. These drill holes have intercepted mineralized and barren rock types. The results reveal that the mobile elements Cs, Rb and Ba tend to be enriched in gold-bearing rock units and depleted in barren rock units. The upper continental crust normalized ratio $((Cs + Rb)/Th)_{UCC}$ is adopted as the alteration index to evaluate and distinguish the possible mineralized zones, with $((Cs + Rb)/Th)_{UCC} > 3$, and barren zones with $((Cs + Rb)/Th)_{UCC} < 3$. The zones of alkali element enrichment present in the Pilar and Três Buracos deposit are up to 100 times greater than the visible alteration halo. The halos identified in the analyzed drill holes are correlated to higher gold grades. The ratio increase towards mineralization and the values $((Cs + Rb)/Th)_{UCC} > 3$ provides a geochemical vector to gold mineralization.

Key words: Archean-Paleoproterozoic Terrane of Goiás; Pilar de Goiás greenstone belt; gold-bearing hydrothermal systems; alkali element mobility; geochemical vector.

1. Introduction

Orogenic gold deposits are a singular class of gold deposits related to tectonic collisions and accretions through time (Groves et al., 1998; Goldfarb et al., 2001). The processes of hydrothermal alteration in orogenic gold deposits are related to the interaction between hydrothermal fluids and wall-rock (Groves et al., 1998; Goldfarb et al., 2005), which are responsible for chemical constituents and heat transfer through the mineral system (Pirajno, 2009; Zhu et al., 2011). An important guide to lead mineral exploration is hydrothermal alteration, because various deposits are classified by their zonation and alteration haloes (Zhu et al., 2011). Factors that affect such alteration mainly include temperature gradients between fluids and wall-rocks and wall-rock compositional variations.

Former authors (Ellis and Green, 1979; Dilles and Einaudi, 1992) recognized that exchange reactions between potassium (K) and sodium (Na) during hydrothermal alteration depends on temperature and proposes that the ratio Na/K in altered rocks and hydrothermal fluids may be adopted to quantify thermal gradients and fluid flow in hydrothermal systems. Previous studies demonstrated that alkali element mobility is associated with gold mineralization in alteration haloes of orogenic gold deposits (Kerrich, 1983). It is known that in some gold deposits hosted in mafic rocks these enrichment assemblages have geochemical halos much larger than the visible alteration, with examples in the Western Australia (Heath and Campbell, 2004; Xu, 1999) and in the Andorinhas greenstone belt, Brazil (Tunussi, 2012). The hypothesis proposes that alkali element enrichment can be used to determine geochemical vectors for exploration in mafic rocks in a greenstone belt setting; however, there is a lack of data regarding felsic and metasedimentary rocks (Heath and Campbell, 2004; Tunussi, 2012).

The Pilar and Três Buracos deposits are hosted in the metasedimentary sequence of the Pilar de Goiás greenstone belt, and the mineralization is directly related to hydrothermal alteration zones. This study is based on petrographic descriptions, lithological modelling and chemical analysis to test the hypothesis that alkali element mobility is disturbed in alteration zones and may be used as a tool to identify fluid flow associated with gold-bearing hydrothermal systems hosted in metasedimentary rocks.

The aim of this work is to show that the ratios of mobile to immobile elements have great discrepancy between barren and mineralized zones in metasedimentary rocks, being a useful technique to generate geochemical vectors to locate new gold prospects in the Pilar de Goiás greenstone belt.

2. Exploration review

Gold was first discovered at Pilar de Goiás in 1736 by fugitive slaves that were later recaptured by João de Godoy Pinto Silveira in 1741, when artisanal gold production started and lasted until 1780. Exploration recommenced in 1972 by Mineração Montita Ltda. and in 2006 Yamana Gold Inc. acquired the exploring rights to start large-scale production in 2013. Since 2018, the company Leagold Mining Corporation has owned the Pilar and Três Buracos operations. The Pilar mine is carried out in underground with 820 m above sea level (300 m deep). The Três Buracos operation is planned to start in 2020 with open pit and future underground potential. The average production in Pilar is 50,000 oz/year and Três Buracos is anticipated to be 20,000 oz/year. An estimate of the total gold production in the Pilar de Goiás greenstone belt is about 30 tons of gold.

The Pilar deposit is one of the most significant gold producers in the Goiás state with a total of measured and indicated resource of 1,191 koz of gold at 2.33 g/t and a total of inferred resource of 2,108 koz at 3.21 g/t as May 31, 2018 (Leagold Mining Corp. 2019 RPA technical report).

3. Geologic setting

The Tocantins Province was formed during the collision of the Amazonian, São Francisco-Congo and Paranapanema cratons (Almeida et al., 1981). It represents a large Pan-African/Brasiliano orogen located in the South American Platform. The province comprises three fold belts: the Araguaia Belt, Paraguai Belt and Brasília Belt **(Figure 3)**, that is positioned in the western limit of the São Francisco Craton (Pimentel et al., 2004).

The evolution of the Archean-Paleoproterozoic Terrane of Goiás is controversial; some authors interpret it as an allochthonous exotic fragment of Archean-Paleoproterozoic crust that has been incorporated to the west of Brasília Belt during the Brazilian Cycle (Jost et al, 2013), while another set of researchers state that the fragment was already incorporated to the Brasília Belt in the Paleoproterozoic (Cordeiro et al., 2017). The limits of the Terrane are exclusively tectonic (Jost et al, 2014). The northern limit of the Archean-Paleoproterozoic Terrane of Goiás with the Mara Rosa magmatic arc is the Mandionópolis shear zone (Pimentel et al., 1997), which is a major low-angle thrust that has positioned the Neoproterozoic rocks of the Santa Terezinha sequence of the Goiás magmatic arc over the

Archean-Paleoproterozoic Terrane of Goiás (Jost and Oliveira, 1991). The southern and eastern limits of the Terrane are in tectonic contact with the metavolcanic and metasedimentary rocks from the Neoproterozoic Brasília Belt, and the western limit is covered by Phanerozoic sediments **(Figure 3)**.

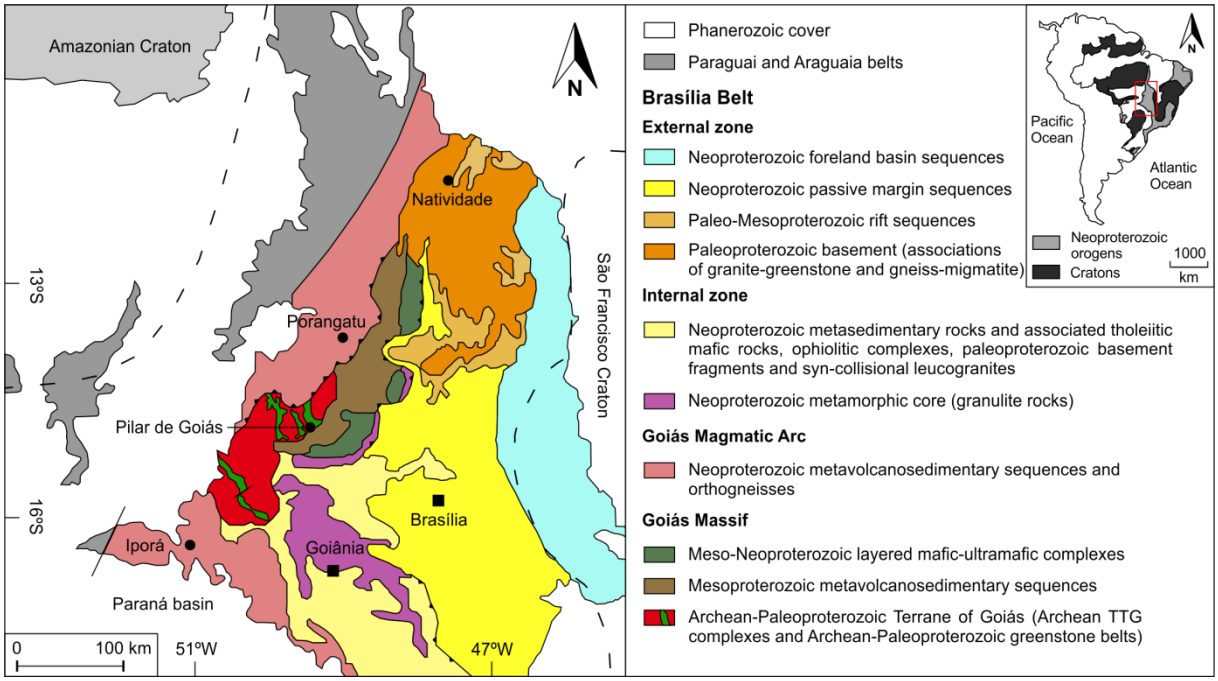

Figure 3. Geological sketch map of the northern segment of the Brasília Belt, Central Brazil (Modified after Pimentel et al., 2004) with the location of the Archean-Paleoproterozoic Terrane of Goiás. Dashed lines show the boundaries of Amazonian and San Francisco Cratons.

The Archean-Paleoproterozoic Terrane of Goiás is composed of five greenstone belts surrounded by six TTG (Tonalite-trondhjemite-granodiorite) terrains. There are four TTG complexes located in the northern (Hidrolina, Moquém, Caiamar and Anta) and two in the southern (Caiçara and Uvá) portion of the Terrane **(Figure 4)**. The greenstone belts occur with similar irregular and elongated morphology that varies from 40 to 100 km long and approximately 6 km wide (Jost and Oliveira, 1991). Each one of the greenstone belts has its own geological and metalogenetic evolution. The northern portion of the Terrane hosts the Pilar de Goiás, Guarinos and Crixás greenstone belts, while Faina and Serra de Santa Rita are positioned in the southern portion. Geochronological data has shown that the evolution of the region is complex with multiple events from Archean to Paleoproterozoic, and Neoproterozoic recycling (Jost et al., 2014).

TTG complexes

The main composition of the TTG complexes is granodioritic to tonalitic and subordinate granitic orthogneisses, with diversity in lithological units, structural framework and magmatic crystallization ages.

There are two stages of magmatism in the northern TTG complexes. The first comprises juvenile poly-deformed granodioritic, granitic and tonalitic orthogneisses of the Caiamar and Hidrolina complexes, and portion of the Anta Complex. The crystallization ages yielded from U-Pb zircon ranges from 2.84 to 2.78 Ga and initial ƐNd values of -1.0 to +2.41. These magmas were probably contaminated by older continental crust as evidenced by the presence of inherited zircon crystals of 3.3 to 3.15 Ga age and a Sm-Nd model age of 3.0 Ga (Queiroz et al., 2008). The second stage is documented in the Moquém Complex and in a portion of the Anta Complex. The crystallization ages based on U-Pb zircon ranges from 2.79 to 2.7 Ga and initial ƐNd value of -2.2 (Queiroz et al., 2008).

Greenstone belts

The northern greenstone belts of the Archean-Paleoproterozoic Terrane of Goiás are composed of lower metavolcanic sequences of metakomatiites and metabasalts overlain by metasedimentary sequences. The general metamorphic grade is greenschist to amphibolite facies. The difficulty in reconstructing the original stratigraphy of the sequences is due to polycyclic deformation, fragmentary state, thickening, which obliterate the primary structures, and the lack of marker horizons (Jost et al., 2014). Original volcanic structures including pillow lavas, spinifex, flux breccia, polyhedral disjunctions and cumulate textures are commonly observed (Teixeira et al., 1981; Kuyumjian and Teixeira, 1982). Banded iron formation, gondite and metachert also may occur intercalated within the metavolcanic rocks. The greenstone belts have crystallization ages of their volcanic protoliths ranging from Archean to Paleoproterozoic. The metabasalts from Pilar de Goiás greenstone belt have U-Pb zircon ages ca. 2.1 Ga, which are compatible to Rhyacian (Jost et al., 2014), while the Sm-Nd isochronic age for the metakomatiites from Crixás greenstone belt is 3.00 ± 0.07 Ga (Fortes et al., 2003).

The greenstone belts have distinct metasedimentary sequences (Jost and Oliveira, 1991; Resende and Jost, 1994; Resende and Jost, 1995; Resende et al., 1998). The source of the clastic content based on isotopic data have suggested a range from the Archean to the Paleoproterozoic (Fortes et al., 2003).

The isotopic data suggest that the metavolcanic rocks of the Pilar de Goiás and Guarinos greenstone belts and the metasedimentary sequences of all greenstone belts are Paleoproterozoic (Rhyacian), while the metavolcanic rocks of the Crixás greenstone belt are Mesoarchean.

Pilar de Goiás greenstone belt

The Pilar de Goiás greenstone belt is located in the northern portion of the Archean-Paleoproterozoic Terrane of Goiás, with approximately 26 km length and 15 km wide, distributed in an irregular N-S trending belt **(Figure 4)** delimited by the Moquém Complex to the west, Hidrolina Complex to the east, Serra da Mesa Group to the south and the Goiás Magmatic Arc to the north **(Figure 3)**. The contact with the TTG complexes Moquém and Hidrolina are tectonic with low- to moderate-angle northeastern-verging shear zones (Jost et al., 2014).

The set of rocks that composes the Pilar de Goiás greenstone belt are basal metavolcanic rocks with komatiitic and tholeiitic affinity and an upper metavolcanosedimentary sequence with several gold occurrences (Jost and Oliveira, 1991). The metavolcanic rocks are more common in the eastern portion of the greenstone belt, while the metasedimentary rocks are predominant in the western area **(Figure 4)**.

The metakomatiites (Córrego Fundo Formation) and metabasalts units (Cedrolina Formation) have been reported by a set of researchers (Teixeira et al., 1981; Kuyumjiann and Teixeira, 1982; Jost and Oliveira, 1991; Jost et al., 1995) and volcanic textures have been described, as cumulatic, pillow lava and spinifex. The metabasalts are mainly tholeiitic and rarely present pillow texture. There are metachert layers, banded iron formation and gondites intercalated with the metavolcanic and a set of mafic dykes and gabbroic sills (Jost et al., 2014).

The metasedimentary rocks are divided into two tectonic units (Resende and Jost, 1995). The lower unit is composed of calcisilicatic rocks (Boqueirão Formation) that tectonically lies above the metabasalts and is interpreted as an allochthonous passive margin sequence. The upper unit is represented by quartz – chlorite schist, carbonaceous schist and metagraywackes (Serra do Moinho Formation), which is known for the numerous gold occurrences (Jost and Oliveira, 1991; Resende and Jost, 1995; Jost et al., 2014), with many former artisanal gold mines distributed throughout the metasedimentary rocks and two mid-tier gold deposits located in the southwest of the greenstone belt: Pilar and Três Buracos mines **(Figure 4)**.

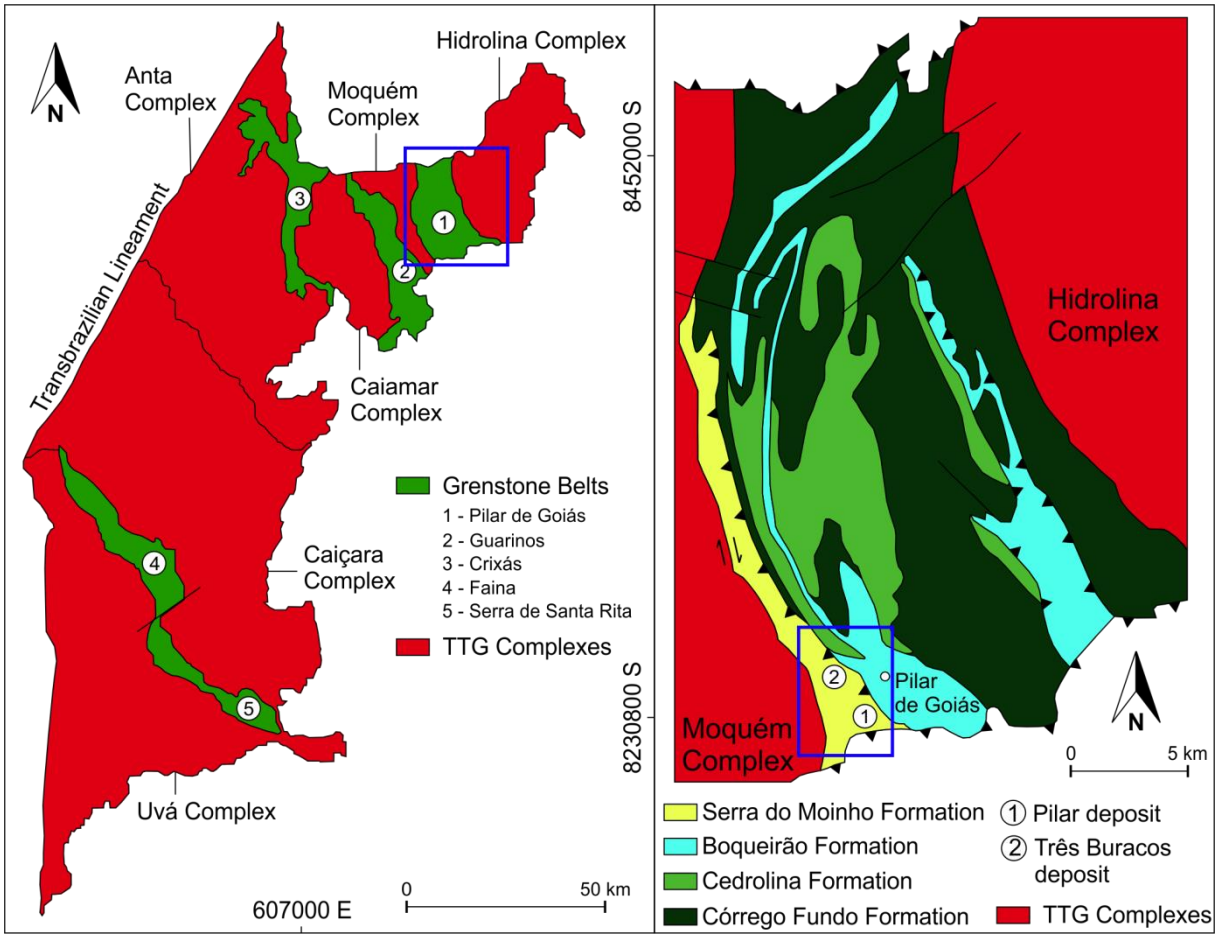

Figure 4. Detailed location of the five greenstone belts of the Archean-Paleoproterozoic Terrane of Goiás and regional geological map of the Pilar de Goiás greenstone belt (Modified after Jost et al., 2014).

4. Geology of Pilar and Três Buracos deposits

4.1. Rocks units

The Pilar and Três Buracos deposits are located in the southwestern portion of the Pilar de Goiás greenstone belt. The area of the deposit is mainly represented by metasedimentary rocks of the Serra do Moinho Formation **(Figure 5)**. The gold mineralization is associated with three mineralized bodies which comprise a set of quartz veins with sulfides and hydrothermal alteration distributed in different rock units of the metasedimentary sequence.

The lithostratigraphic sequence at the deposits comprises six individual units belonging to the Serra do Moinho Formation. The units are similar and due to the lack of preserved outcrops and the difficulty in recognizing weathered schist in the field, diamond drill holes supported the interpretation to define the lithological contacts **(Figure 6)**. The lithostratigraphic units are described below from bottom to top.

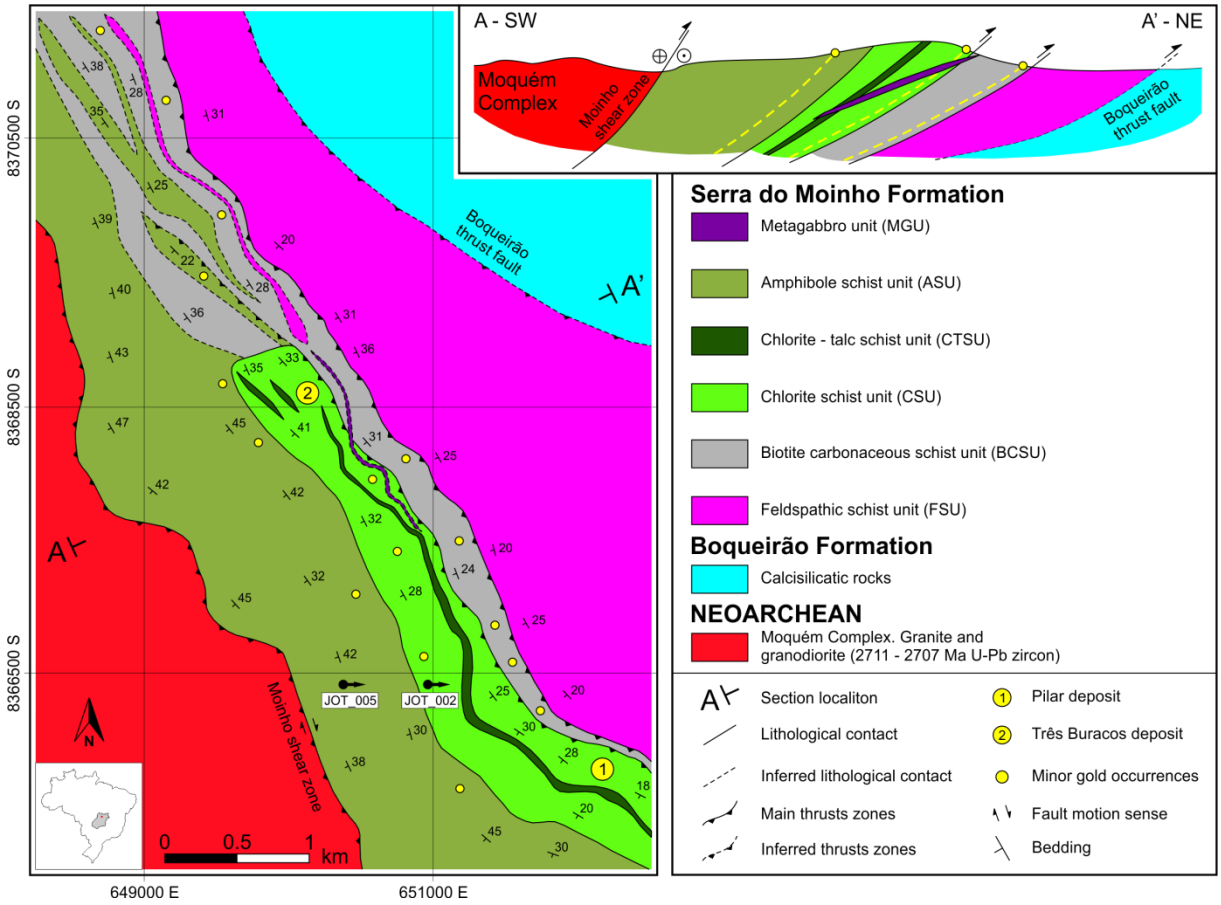

Figure 5. Geological map and cross section of the southeastern part of the metasedimentary sequence of the Pilar de Goiás greenstone belt, including Pilar and Três Buracos gold deposits and minor gold occurrences. The representative cross section shows the relationships between main stratigraphic units and major faults.

Feldspathic schist unit (FSU)

The lowermost unit of the Serra do Moinho Formation is composed of a sequence of feldspathic schist with millimeter to centimeter scale banding characterized by the alternation of quartzofeldspathic and biotite-rich layers **(Figure 6A)**. The thickness of the unit is approximately 70 meters and outcrops from the north to the southeast portion of the Três Buracos deposit **(Figure 5)**. The lower contact with the Boqueirão Formation is tectonic and upper contact is abrupt.

The schist is composed of variable amounts of quartz (40-60%), biotite (15-35%), muscovite (5-20%), chlorite (3-10%) and plagioclase (<5%), with subordinate garnet (<5%). The texture is characterized by alternation of granoblastic and lepidoblastic texture with milimetric intercalation between the domains **(Figure 7A)**.

The tectonic foliation is characterized by a spaced, anastomosing schistosity, defined by a

preferential orientation of biotite, muscovite and chlorite. Millimeter to centimeter scale quartz and carbonate veins are common in the hydrothermal zones.

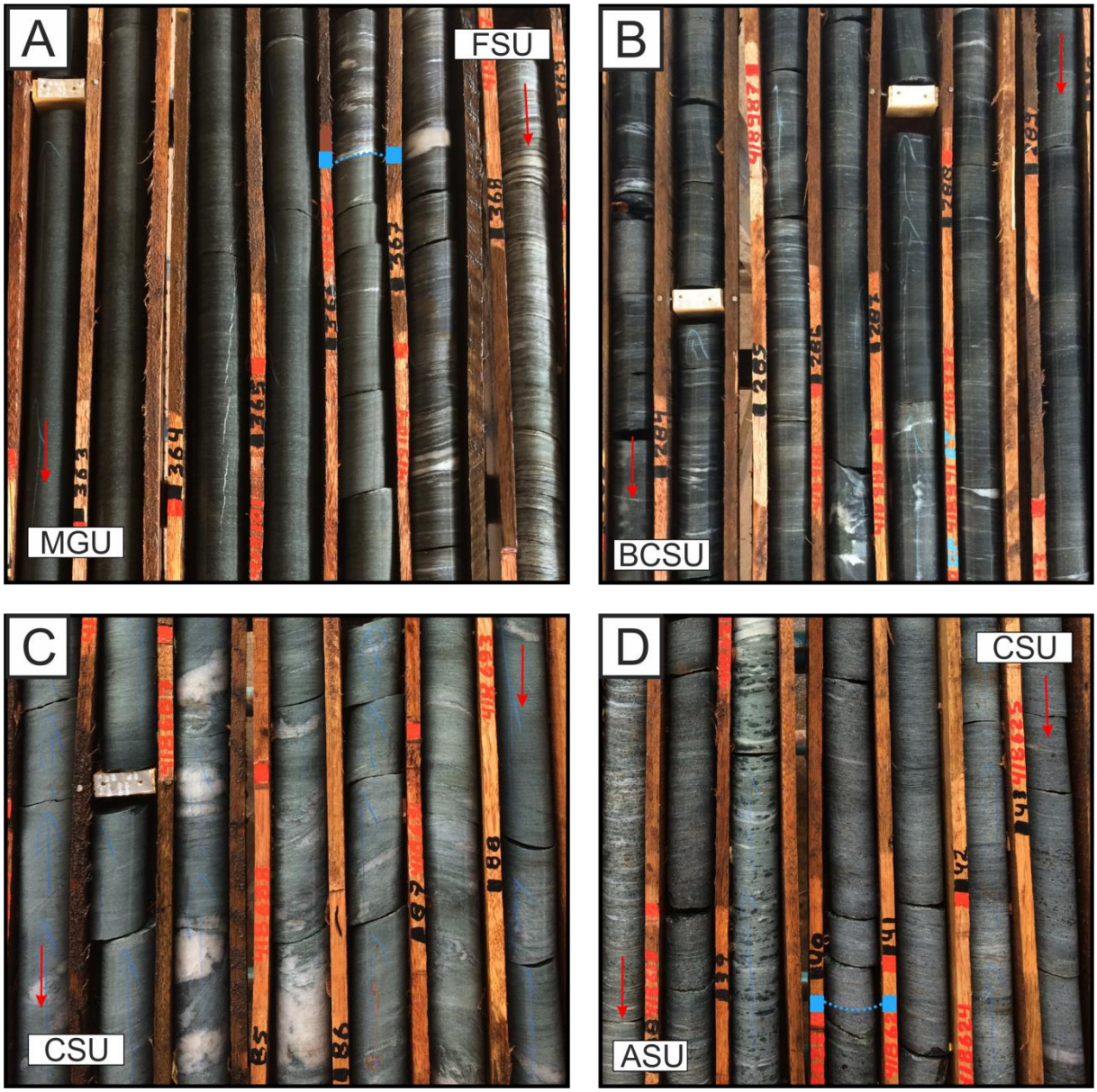

Figure 6. Main units of the Serra do Moinho formation. Red arrows indicate the surface direction and blue dashed lines determine lithological contact between units. (A) Millimeter to centimeter scale banding of the feldspathic schist unit (FSU) showing abrupt contact with metagabbro unit (MGU). (B) Biotite carbonaceous schist unit (BCSU) showing intercalation of black bands of carbonaceous matter and lighter bands of quartz and muscovite-rich layers. (C) Chlorite schist unit (CSU) with greenish chlorite-rich layers intercalated with lighter quartz-rich layers. (D) Amphibole schist unit (ASU) represented by the medium-grained amphibole crystals; abrupt contact with chlorite schist unit (CSU).

Biotite carbonaceous schist unit (BCSU)

The biotite carbonaceous schist unit **(Figure 6B)** comprises as much as 70% of carbonaceous matter **(Figure 7B)** intercalated with thin layers of quartz (20-45%), biotite (5-35%), muscovite (5-20%), chlorite (3-15%) and occasionally plagioclase (<5%). The unit occurs as a layer from the north to the south of the Três Buracos deposit **(Figure 5)**, which thickness varies from 5 m in the southeast to nearly 150 m in the north, and both lower and upper contacts are abrupt.

The rock is dark gray fine-grained and displays diffuse parallel banding defined by the presence of lepidoblastic texture with brownish bands of biotite and granoblastic texture with predominance of quartz in colorless bands. Black bands of carbonaceous material occur within these two domains. Also, it is common to find sparse syn-tectonic garnet porphyroblasts with pressure shadow usually filled with phyllosilicates.

Chlorite schist unit (CSU)

The chlorite schist unit outcrops from the southeast to the central portion of the deposit **(Figure 5)**. The rock is light gray fine-grained and displays diffuse parallel banding with colorless bands of quartz and plagioclase intercalated with light green bands of chlorite and muscovite **(Figure 6C)**. Porphyroblasts of garnet are also commonly found composing the metamorphic assembly. The unit is about 100 m thick and both lower and upper contacts are abrupt **(Figure 6D)**.

The unit is composed of quartz (40-60%), muscovite (10-40%), chlorite (10-25%), biotite (10-20%), carbonate (<10%), plagioclase (<5%) and subordinate garnet (<5%) distributed throughout de rock **(Figure 7C)**. The presence of calcite is limited to quartz veins associated with alteration zones **(Figure 7D)**. The weak magnetism is due to the presence of sparse magnetite randomly distributed throughout the rock. The tectonic foliation is characterized by spaced and anastomosing schistosity, defined by a preferential orientation of chlorite and biotite.

Amphibole schist unit (ASU)

The uppermost unit of the Serra do Moinho Formation occurs in the southwest of Três Buracos and Pilar deposits **(Figure 5)**. It ranges from 100 to about 200 m thick, with the

lower contact abrupt and the upper contact with the Moquém Complex tectonic. Metric layers of carbonaceous schist occur intercalated in this unit, rarely related to low grade gold mineralization. The upper part of the unit commonly occurs metric layers of sericite schist, quartzite and gondite.

The rock is light gray-greenish fine-grained and composed of a sequence of millimeter scale felsic bands **(Figure 6D)** of quartz (20-50%), muscovite (10-30%) and plagioclase (<10%), and greenish bands of amphibole (20-50%) and chlorite (10-40%). The fabric has grano-lepidoblastic and poikiloblastic textures. The tectonic foliation is determined by the preferred orientation of biotite and amphibole **(Figure 7E)**, while the quartz and micaceous domains form millimeter scale intercalation **(Figure 7F)**. Similarly to CSU, calcite occurs associated with quartz veins. There are two types of garnet crystals. The first type of garnet is represented by irregular-shaped medium-grained rotated porphyroblasts with pressure shadow filled with quartz, biotite, chlorite and sulfides that disturb the foliation; and the second type are typically euhedral medium-grained late tectonic porphyroblasts. It is suggested that the first type of garnet composes the metamorphic assembly and the second type is late-stage formed during percolation of hydrothermal fluids. The amphiboles occur as subhedral medium-grained prismatic porphyroblasts oriented along the main foliation, occasionally rotated, with inclusions of quartz, carbonate and sulfides. The mineral assemblage near the mineralized veins includes fine-grained muscovite, biotite constantly altered to chlorite, arsenopyrite, chalcopyrite and pyrite.

Chlorite – talc schist unit (CTSU)

This unit occurs as a thin continuous layer within the CSU that varies from a 10 centimeters to 30 meters thick and is present from the southeast to the northwest of the Pilar and Três Buracos deposits **(Figure 5)**. The schist is primarily composed of talc (20-50%) and chlorite (10-40%), with subordinate tremolite (10-20%), biotite (10-20%), quartz (<10%), feldspar (<10%) and pyrite (<5%). The lower and upper contact are abrupt.

The rock is fine-grained light-green and displays granoblastic and lepidoblastic textures. The tectonic foliation is defined by the preferential orientation of talc, chlorite, and rarely biotite porphyroblasts. The granoblastic domain is defined by the presence of feldspar and quartz occurring intercalated with the lepidoblastic domain, which is composed of talc and chlorite. The interpretation regarding this unit suggests an ultramafic flow or sill metamorphosed under upper greenschist to lower amphibolite facies.

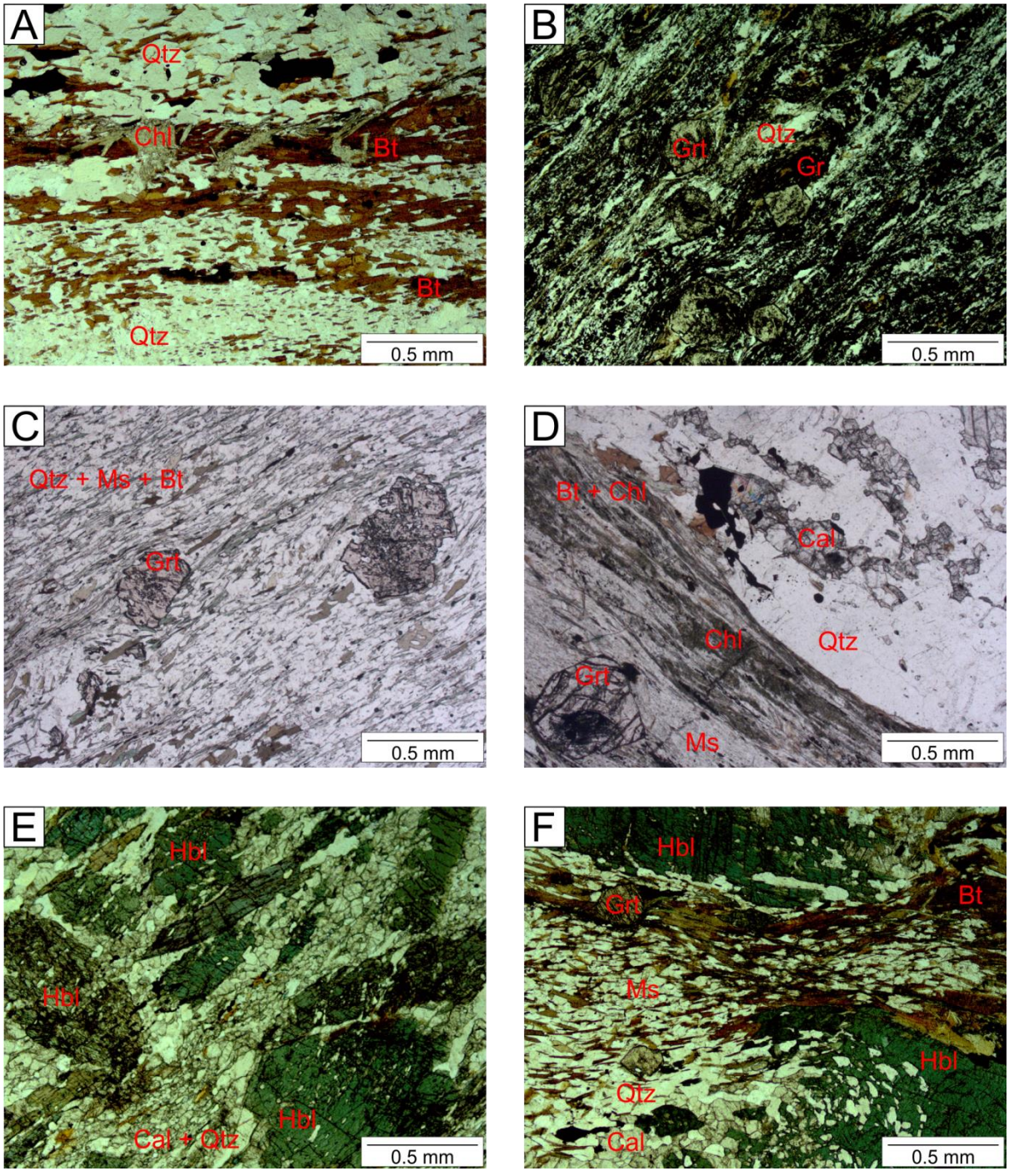

Figure 7. Photomicrographs illustrating the rock types of the Pilar and Três Buracos gold deposits: A – Feldspathic schist unit (FSU). B – Biotite carbonaceous schist unit (BCSU). C and D – Chlorite schist unit (CSU). E and F – Amphibole schist unit (FSU). (A) sample RTB010-14, millimeter scale alternation between quartz and biotite/chlorite rich layers. (B) sample RTB010-8, carbonaceous matter (black) intercalated with quartz-rich layers and rotated syn-tectonic garnet porphyroblasts with pressure shadow. (C) sample RTB002-2, distal sample of CSU, represented by milimetric intercalation of oriented quartz, muscovite and biotite, and metamorphic garnet porphyroblasts. (D) sample RTB002-5, presence of calcite associated with quartz veins and late stage garnet in alteration zone. (E) sample RTB010-1, rotated amphibole porphyroblasts surrounded by

quartz, carbonate and biotite. (F) sample RTB010-7, oriented biotite and amphibole crystals with millimeter scale intercalation of quartz and biotite domains. Presence of late stage garnets and calcite associated with quartz veins.

Metagabbro unit (MGU)

There are a set of meta-igneous rocks positioned subparallel to the original bedding of metasedimentary sequence **(Figure 5)**. The thickness of these bodies varies from 5 centimeters to 40 meters. The weathering has completely obliterated the metagabbro outcrops so the only manner to interpret this unit is by analyzing drill cores. The igneous texture is preserved and prevails over the metamorphic texture.

The rock is dark green medium-grained, foliated, weakly magnetic, displays dark green crystals of hornblende, colorless crystals of plagioclase and brown laths of fine-grained biotite. It rarely presents plagioclase phenocrysts (1 to 5 cm), which are relicts from the original igneous porphyritic texture, which are altered to secondary minerals as carbonates.

4.2. Geological model and deposit geometry

The structural framework of the deposit is characterized by a fold and thrust system formed by a series of sub-parallel thrust sheets, delimited by the Moinho shear zone and Boqueirão fault **(Figure 5)**. The thrusts are defined by NW oriented low-angle shear zones. Kinematic indicators show NE reverse-oblique sense of movement. The east verging direction is determined by the isoclinal and recumbent folds associated with the thrust system (Pulz, 1995; Jost et al., 2014).

Gold mineralization is structurally controlled and the deposits have characteristics that suggest a brittle-ductile transition of the mineralized structures (Pulz et al., 1995; Jost et al., 2014). The mineralized zones are composed by a set of intercalated quartz veins as thick as 1.5 meter parallel to the main mylonitic foliation.

The Três Buracos lithological model was created based on 89 drill holes (Appendix A) data acquired from more than ten years of drilling **(Figure 8)**. The interpretation was supported by fieldwork activity, geological description and interpretation of 20 cross sections with slices of 100 meters.

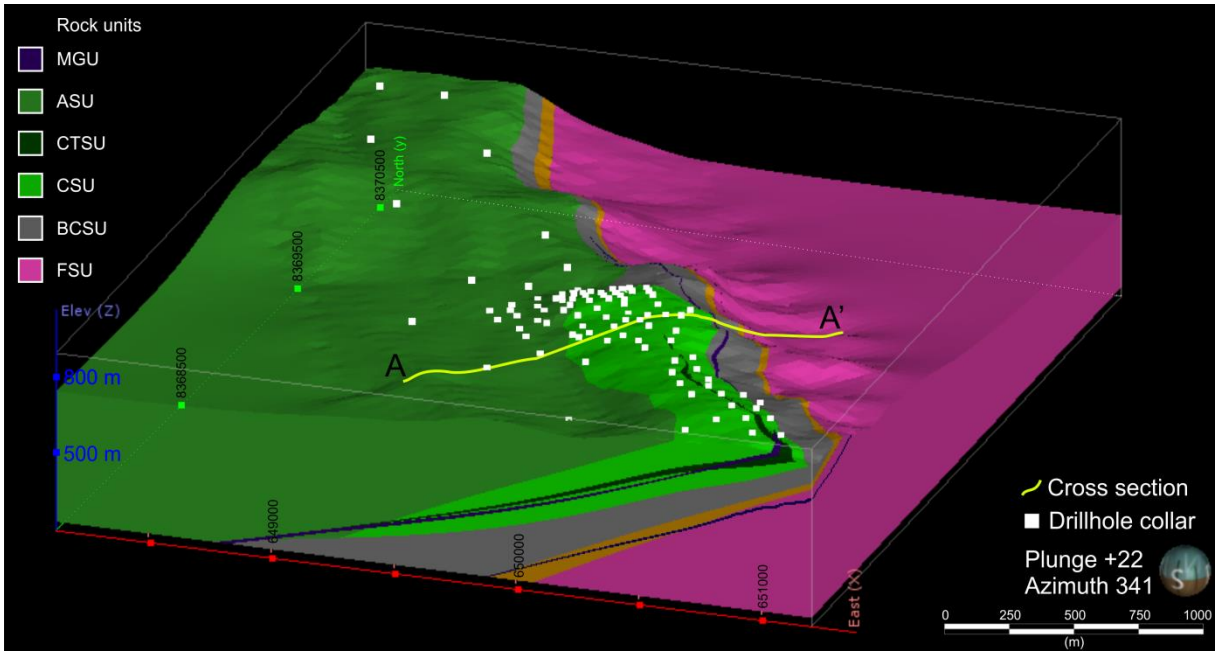

Figure 8. Três Buracos geological model and cross section location. Rock units: Feldspathic schist unit (FSU), biotite carbonaceous schist unit (BCSU), chlorite schist unit (CSU), amphibole schist unit (ASU), chlorite – talc schist unit (CTSU) and Metagabbro unit (MGU). The orange layer modeled represents the geochemical vector around the main mineralization. The geological software to create the model is Leapfrog Geo 3.1. The drill holes JOT_002 and JOT_005 are located to the south of the model and are not included on this diagram.

The representative cross-section A-A' **(Figure 9)** is located at the center of the Três Buracos deposit. Four drill holes (JD_503, TB_019, JOT_129 and JD_536) were selected to represent the geometry of the rock units. All of the metasedimentary units are gently dipping to southwest. The mineralized levels are hosted in the metasedimentary rocks occurring parallel to the tectonic foliation. The CTSU occurs within the CSU with abrupt contact and its position fluctuates from the bottom to the top of the layer. The positioning pattern of the MGU is subparallel crosscutting the main foliation with abrupt contact and angles from 10º to 15º. They are represented by single or multiple continuous layers that can be followed for 5 kilometers.

The mineralized levels are named from the bottom to the top: HG1, hosted in the BCSU; HG2, hosted in the CSU; and HG4, hosted in the ASU. The levels HG1, HG2 and HG4 have sublevels; however, for the purposes of this study they were grouped due to the difficulty in demonstrating these sublevels individually.

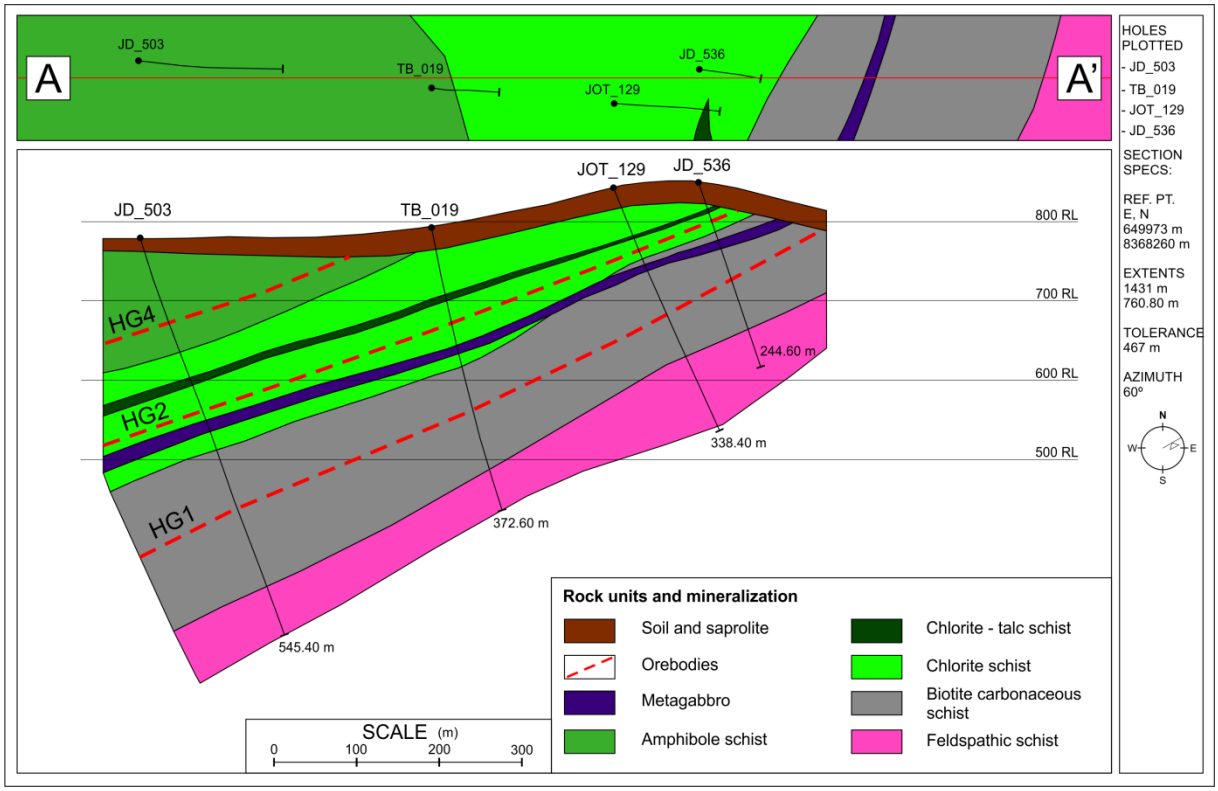

Figure 9. Três Buracos cross-section located in the central area of the deposit. The upper part of the cross-section diagram shows a plan view with drill holes location, survey data and geological map, and on the right side a box provides the cross-section specs and location. The cross-section comprises the six units of the Serra do Moinho Formation, from the base to the top: feldspathic schist unit (FSU), biotite carbonaceous schist unit (BCSU), chlorite schist unit (CSU), amphibole schist unit (ASU), chlorite – talc schist unit (CTSU) and metagabbro unit (MGU).It is also indicated the approximate position of the mineralized levels HG1, HG2 and HG4.

5. Gold mineralization

5.1. Style of mineralization

Gold mineralization at Três Buracos and Pilar deposits is associated with quartz veining **(Figure 10)**. The gold is free in the quartz veins, commonly occurring as gold nuggets, and usually accompanied with sulfides (<5 vol.%). The gold-mineralized quartz veins orebodies are parallel to the main mylonitic tectonic foliation and positioned in NW-SE shear zones **(Figure 10A)**.

Sulfides can be euhedral to anhedral, aligned to the tectonic foliation or randomly distributed and up to 1 cm. Strong hydrothermal alteration replaces the rock's mineral assemblage to biotite, muscovite, chlorite and garnet around the fault-fill quartz veins **(Figure 10B)**. The gold-bearing quartz veins are smoky to milky and slight translucent, with sparse

sulfides within and around the veins. The full list of association of sulfides and hydrothermal alteration with the orebodies is summarized in the next section. The presence of barren post-gold milky opaque quartz veins discordant to the tectonic foliation up to 5 m thick is common.

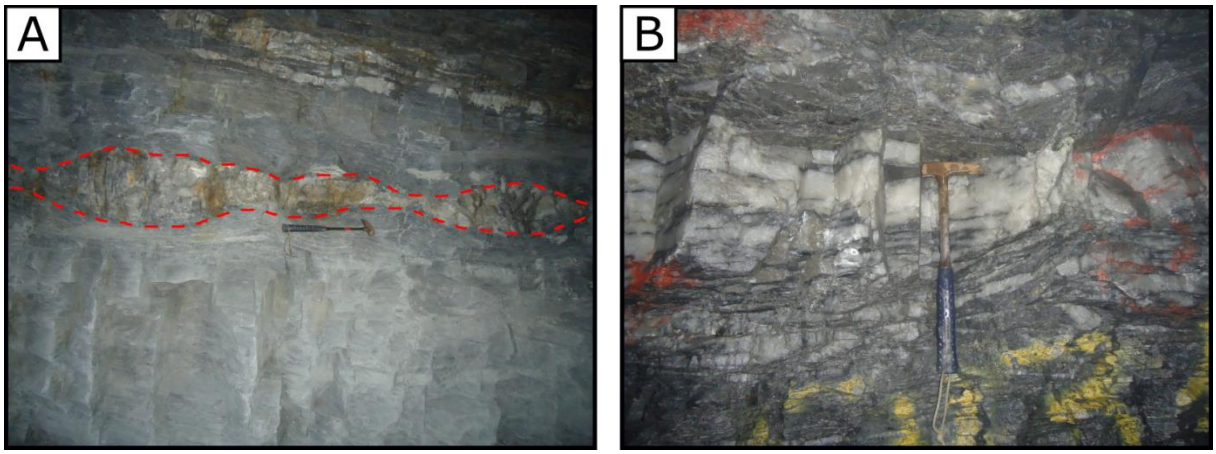

Figure 10. Pilar underground mine veining system in the BCSU. The ore thickness varies from 5 to 60 cm. (A) Boudinage veins parallel to the mylonitic foliation. Red dashed lines shows the limit of the quartz veins. (B) Mineralized fault-fill veins surrounded by strong hydrothermal alteration.

There are three main orebodies at the Pilar and Três Buracos deposits: HG1, HG2 and HG4 **(Figure 9)**. These orebodies are continuous mineralized structures over >5.8 km in surface from Pilar to Três Buracos deposit.

Orebody HG1

The HG1 is hosted in the BCSU positioned in a low-angle shear zone and is the main orebody. The vein system is divided into the sublevels HG1.1, HG1.2, HG1.2A and HG1.3. The gold occurs free within the quartz veins and nearby arsenopyrite, galena and sphalerite with average grade of 3.5 grams per ton. The thickness ranges from 10 cm to 2.5 m (average 1.2 m) and the extent from the surface to the deepest drill hole interception is approximately 5 km, while the strike length is 5.6 km.

The most abundant sulfide in HG1 is arsenopyrite, which occurs as fine-grained (<1 mm) oriented laths or irregular forms distributed throughout the quartz veins and the proximal zone. Pyrrhotite is a common sulfide present in HG1 with fine-grained irregular shape generally forming crystal aggregates in quartz veins and layers aligned parallel to the tectonic foliation around the ore. The sulfides galena and sphalerite occur as sparse subhedral fine-grained crystals and are rare; however, they are the best tracers for higher gold grade. The

subordinate presence of pyrite and chalcopyrite is not regular and apparently there is no directly correlation to gold mineralization.

Orebody HG2

The HG2 orebody is hosted in the CSU. The sublevels HG2.1, HG2.2, HG2.3 and HG2.4 are discontinuous. Contrasting to HG1, gold is strongly associated with pyrrhotite and the grade average is about 2.5 grams per ton. The thickness varies from 5 cm to 2.0 m (average 1.0 m) and the extent from the deepest drill hole interception to the surface is approximately 3 km. The strike length is approximately 5 km, however with many unmineralized gaps.

The quartz veins of the HG2 orebody and sublevels are easily recognized due to the abundance of pyrrhotite, which occurs as fine-grained (<1 mm) anhedral crystals that commonly form aggregates in the vein and proximal zone. The pyrrhotite is weakly magnetic and directly associated with higher gold grades; however, samples without any sulfide may return positive values for gold content. The presence of pyrite and chalcopyrite is common however do not necessarily represent higher gold content.

Orebody HG4

The HG4 orebody is hosted in the ASU, which is the least continuous and more erratic level in terms of gold grade, with an average of 1.0 gram per ton. The thickness varies from 5 cm to 1.5 m (average 80 cm) and is not possible to define the extent from surface to the deepest drill hole interception due to countless unmineralized gaps. The longest continuous mineralized extent is approximately 300 m. There is only one sublevel with similar characteristics named HG4.1, which is hosted in layers of carbonaceous schist that occurs intercalated with the ASU.

The quartz veins in HG4 and HG4.1 range from 1 centimeter to 1 meter and are distant from each other. Gold nuggets are common and the dominant sulfide in HG4 is subhedral pyrite with rare occurrence of pyrrhotite and arsenopyrite, while in the sublevel HG4.1 the main sulfide is arsenopyrite, which is euhedral and oriented to the tectonic foliation, with subordinate subhedral pyrrhotite and pyrite.

5.2. Hydrothermal alteration

Three zones of hydrothermal alteration were identified at Três Buracos deposit and are presented in **Figure 11**, the distal, proximal and vein hydrothermal zones. Distal hydrothermal alteration zone represents the metamorphic assemblage, proximal is regarding to the alteration up to 5 meters from the mineralization and the vein alteration zone is the centimeter scale alteration zone at the mineralization itself. The alteration zone is roughly tabular and accompanies the structure that hosts the mineralization. The amount of sulfides and veins increases substantially from distal to vein-proximal alteration zones. The alteration halos occur around the veining system and slightly overprint the regional metamorphic assemblage, showing mineralogical zonation around the quartz veins. The combination of drill hole and petrographic description determined different mineral associations for each mineralized level.

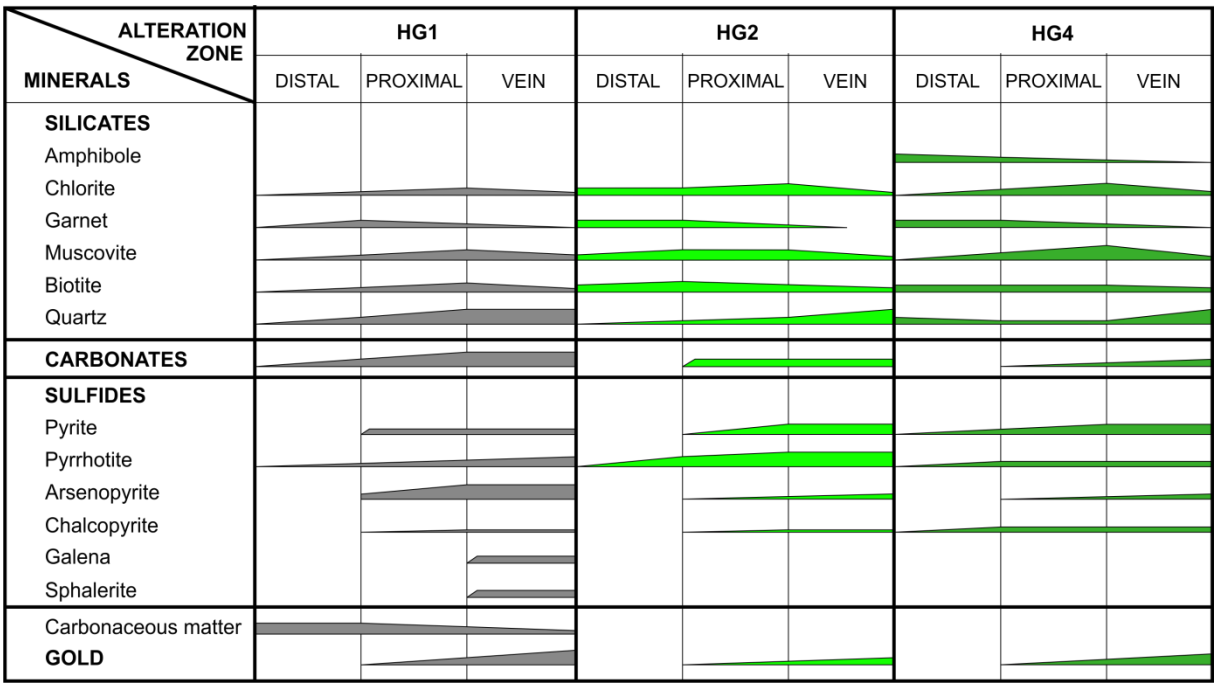

Figure 11. Summary of mineral associations of each mineralized level for Pilar and Três Buracos deposit. The HG1 level is hosted in the BCSU, the HG2 is hosted in the CSU and the HG4 is hosted in the ASU. The colors adopted are the same for the units in which they are hosted in the cross section shown in Figure 9.

These criteria suggests that all rock types are subjected to hydrothermal alteration and the zone is defined whether it is near the mineralized quartz veins or not. The distal, proximal and vein mineral assemblages are different for the rock units **(Figure 12, 13 and 14)**.

The mineral association for HG1 level is summarized in **Figure 11**. The proximity to mineralized veins result in increasing content of biotite, carbonate, garnet, arsenopyrite, pyrrhotite and pyrite, and decreasing proportion of organic matter. The hydrothermal

alteration is mainly represented by quartz and carbonate veins in the proximal zones, which ranges from millimeter to centimeter scale length. Biotite, muscovite and chlorite near the mineralized veins associated with hydrothermalism are fine-grained bordering the quartz veining system **(Figure 12A)**. Garnet is present in the proximal hydrothermal zone **(Figure 12B)**, which is represented by medium-grained rotated porphyroblasts commonly with pressure shadow and inclusions.

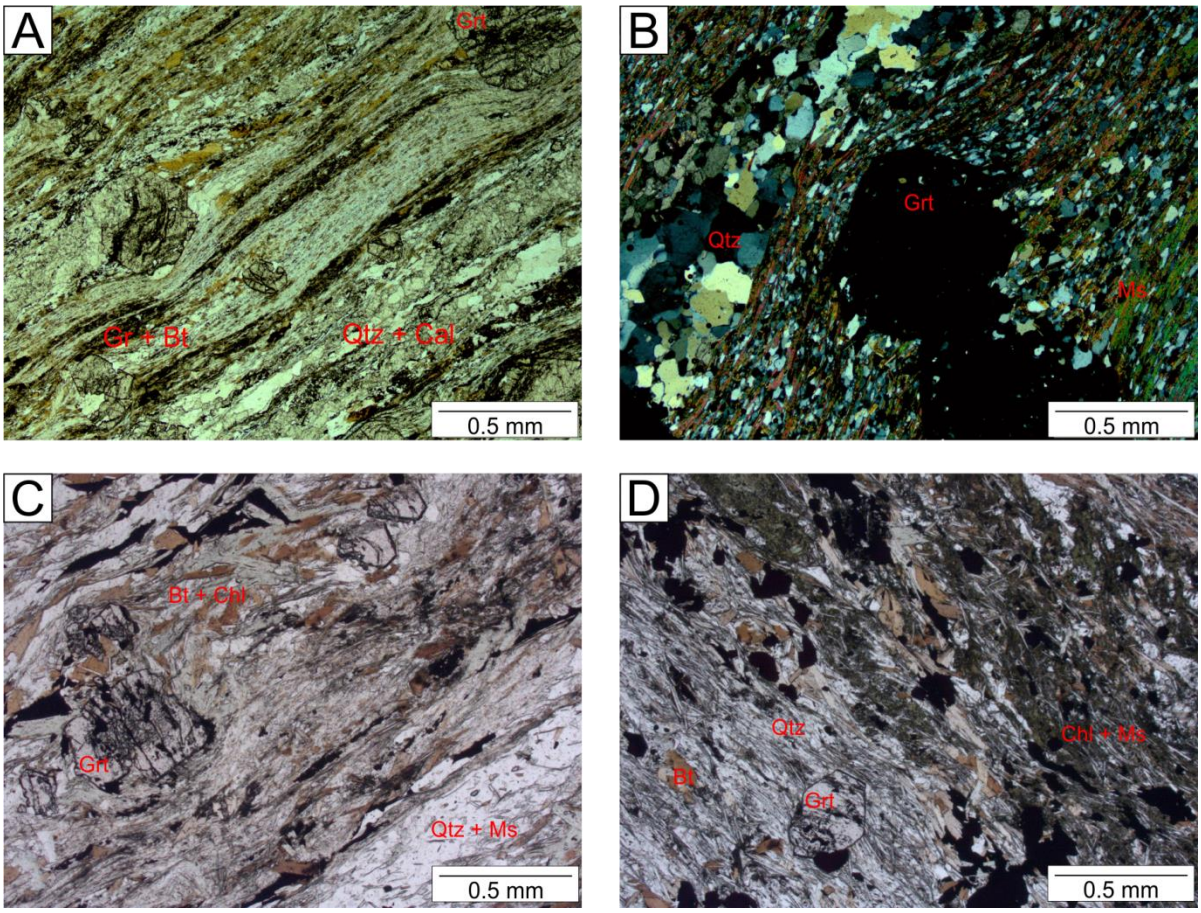

Figure 12. Photomicrographs representing the hydrothermal alteration of the HG1 and HG2 level: A and B – HG1 level; C and D – HG2 level. (A) Classic HG1 proximal zone. The proportion of carbonaceous matter has decreased in comparison with the distal zone, porphyroblasts of garnet are rotated with pressure shadow and inclusions, quartz-carbonate veins are surrounded by muscovite and biotite, which is commonly altered to chlorite (Sample RTB010-8). (B) HG1 ore with quartz vein surrounded by biotite, chlorite, muscovite, garnet porphyroblasts and minor recrystallized quartz grains (sample RTB010-9). (C) Representative thin section of HG2 level. Hydrothermal alteration represented by micaceous minerals near quartz vein. Biotite is partially replaced to chlorite. Opaque minerals are pyrrhotite and arsenopyrite within the micaceous layer. Late garnet porphyroblasts are rotated along the mylonitic foliation (sample RTB002-5). (D) Strong hydrothermal alteration represented by millimeter scale intercalation of micaceous and quartz-rich layers. Biotite is replaced by muscovite and chlorite. Garnet porphyroblasts are euhedral and occur rotated along the mylonitic foliation (sample RTB002-3).

The gold in the mineralized veins of HG1 level is surrounded by arsenopyrite. Other sulfides as pyrrhotite, galena, sphalerite, pyrite and chalcopyrite are also common **(Figure 13)**. Arsenopyrite can occur as fine-, medium- and/or coarse-grained, euhedral to subhedral crystals, forming parallel bands and generally associated to gold **(Figure 13A)**. Pyrrhotite forms fine to medium-grained anhedral oriented crystals concentrated in bands. It was observed intergrown and replacing with both arsenopyrite and pyrite, suggesting that it has crystallized later **(Figure 13B, 13C and 13D)**. Galena occurs as fine- to medium-grained subhedral oriented crystals, intergrown and surrounding pyrrhotite, sphalerite and chalcopyrite, apparently replacing them and suggesting later crystallization **(Figure 13B and 13D)**. Sphalerite forms medium- to coarse-grained, subhedral to anhedral oriented crystals, commonly intergrown and replacing pyrrhotite **(Figure 13B)**. Pyrite occurs as medium- to coarse-grained, subhedral to anhedral crystals forming parallel bands **(Figure 13C)**. Chalcopyrite occurs as fine-grained anhedral crystals commonly intergrown and replacing arsenopyrite, and sometimes being replaced by galena **(Figure 13D)**.

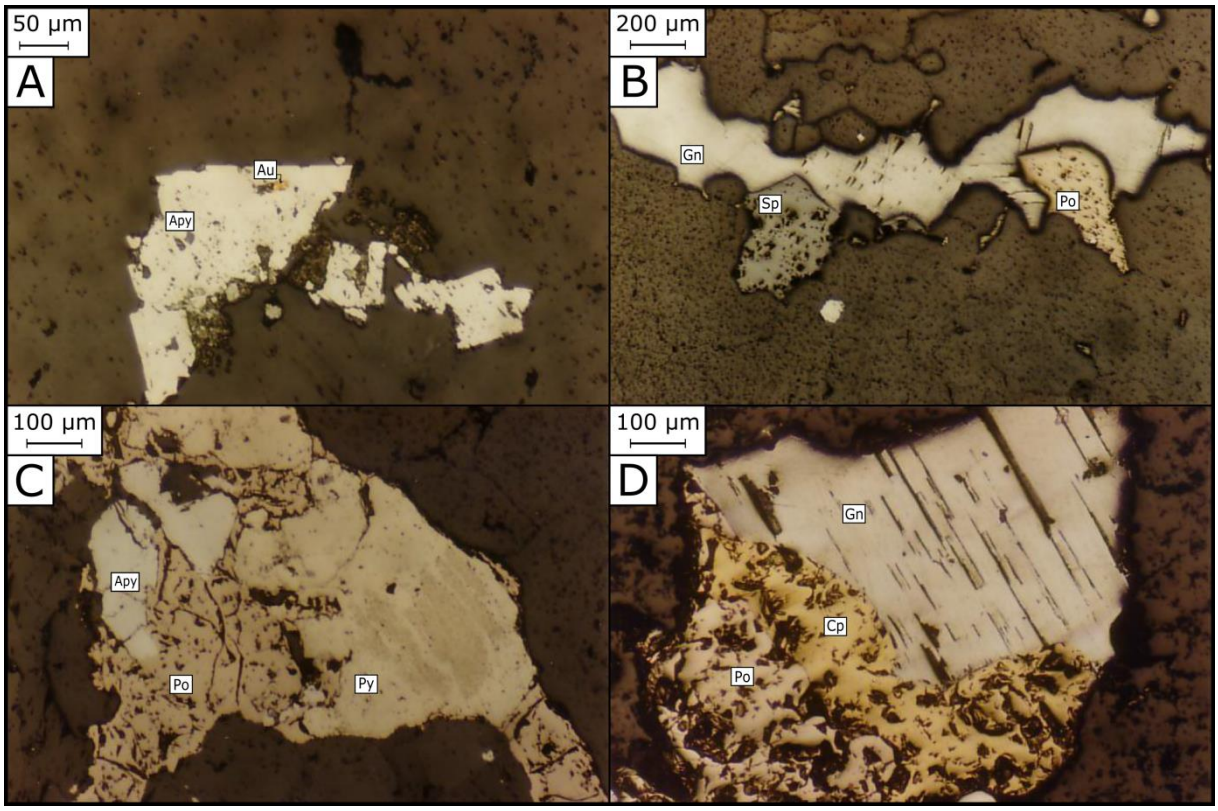

Figure 13. Photomicrographs of polished section of sulfides and native gold present in the HG1 mineralized level. (A) Native gold (Au) in arsenopyrite (Apy; sample PEX-60-008A). (B) Galena (Gn) surrounding and replacing sphalerite (Sp) and pyrrhotite (Po; sample PEX-60-08A). (C) Pyrrhotite (Po) surrounding and

replacing pyrite (Py) and arsenopyrite (Apy; sample PEX-60-08A). (D) Galena (Gn) surrounding chalcopyrite (Cp) and chalcopyrite (Cp) surrounding pyrrhotite (Po; sample PEX-60-08B).

The mineral alteration assemblage of HG2 is presented in **Figure 11**. Carbonaceous matter is totally absent in this alteration zone. The hydrothermal fine-grained muscovite, biotite and chlorite occur as laths bordering the mineralized veins, while calcite is associated with quartz veins and more present in the proximal and vein zone. Chlorite is commonly replacing biotite and muscovite **(Figure 12C and 12D)**. The mineralized quartz veins are associated with pyrrhotite, arsenopyrite, pyrite and chalcopyrite. Pyrrhotite is the most common sulfide and is the best tracer for gold mineralization, occurring as aggregates 10 centimeters near the quartz veins within the alteration minerals. Arsenopyrite and pyrite are less common and occur as rotated subhedral crystals bordering hydrothermal alteration. Chalcopyrite is rare and there is no direct correlation to mineralization.

The minerals that compose the hydrothermal alteration zone of the HG4 level are summarized in **Figure 11**. The proximal mineral assemblage consists of lesser amount of amphibole and increased amount of rotated garnets **(Figure 14A and 14B)**. The biotite and muscovite crystals occur bordering the quartz veins and are generally partially or completely altered to chlorite **(Figure 14C and 14D)**. The presence of chlorite can be as a pervasive alteration or altering biotite crystals, resulting in substitution textures with diffuse or interdigitated contact **(Figure 14E)**. The occurrence of carbonate and arsenopyrite are secondary **(Figure 14F)**.

6. Geochemistry

Sampling and analytical methods

The 469 samples analyzed are from two diamond drill holes in the Pilar de Goiás greenstone belt. Both drill holes are located in the Serra do Moinho Formation and the drilling was undertaken in 2006 to explore the northern area of Três Buracos deposit. There are approximately 1200 drill holes at the Pilar and Três Buracos deposits; however, since it was not the company's interest to do complete multielements analysis, just these two drill holes were analyzed for the required elements to reproduce the method of this work. The exploration department is temporarily closed and the access to resample the drill holes is limited. The gold grades and elements analysis for the selected drill holes are shown in Appendix B.

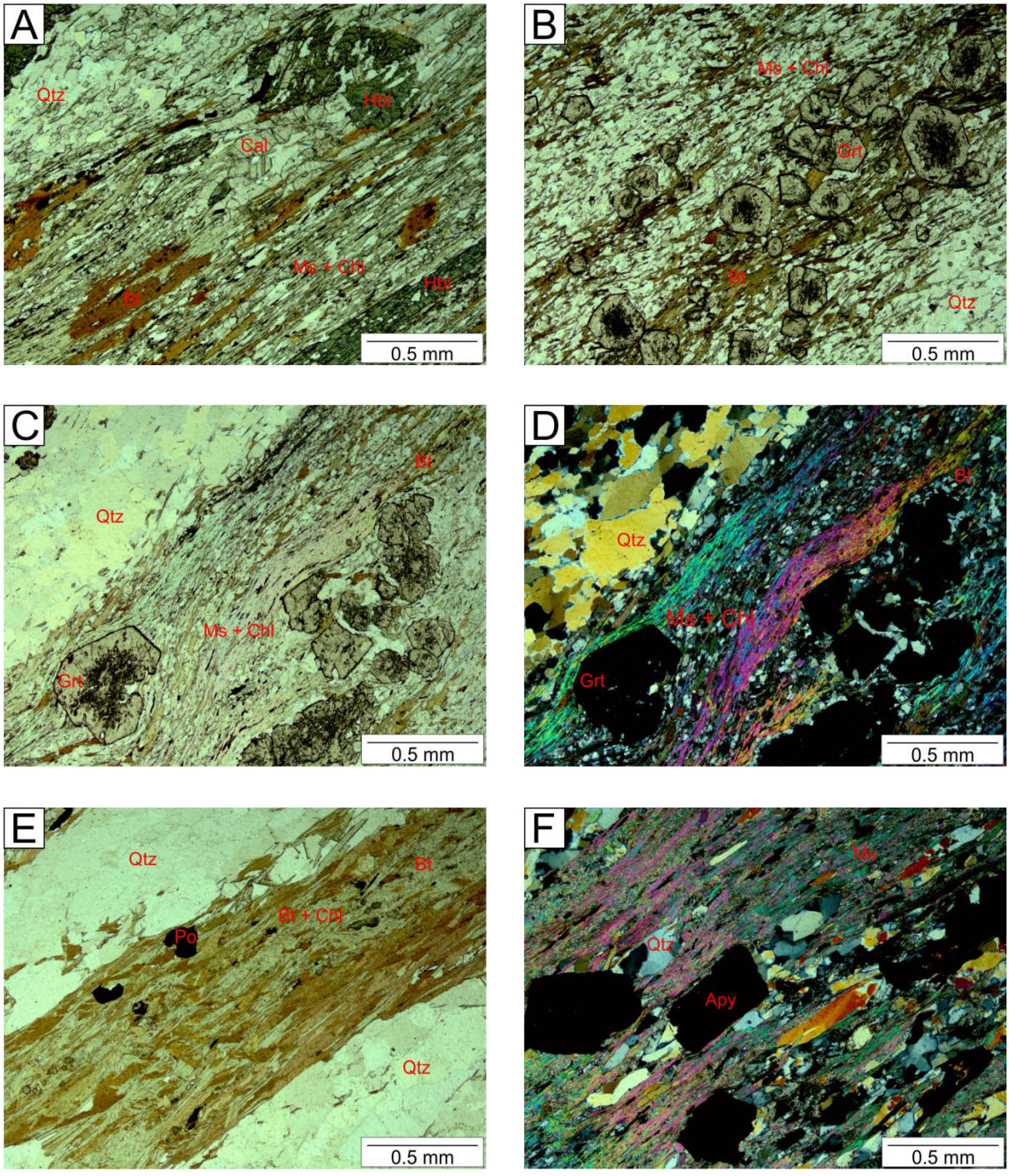

Figure 14. Photomicrographs representing the hydrothermal alteration of the HG4 level. (A) Hornblende crystals in the proximal zone. Moderate hydrothermal alteration near the quartz vein, represented by the presence of calcite, muscovite, and biotite being replaced by chlorite (sample RTB010-1). (B) Late stage rotated garnets porphyroblasts surrounded by quartz, muscovite, biotite and chlorite (sample RTB010-2). (C) Strong hydrothermal alteration near quartz vein represented by rotated garnet porphyroblasts surrounded by pyrrhotite, muscovite and biotite being replaced by chlorite (sample RTB010-5B). (D) Cross polarized light of image (C; sample RTB010-5B). (E) Micaceous layers near mineralized quartz veins. Biotite is replaced by chlorite in the proximal zone (sample RTB010-5C). (F) Millimeter-scale intercalation between mineralized quartz veins and

micaceous minerals (mainly muscovite, rare biotite and chlorite) in the ore zone. Opaque minerals are subhedral to euhedral arsenopyrite crystals oriented along the mylonitic foliation (sample RTB010-4).

The samples are from the drill holes JOT_002 and JOT_005 **(Figure 5)**. The drill hole JOT_002 was analyzed from 23.14 to 250.06 m depth, resulting in 246 samples, while the drill hole JOT_005 was analyzed from 103.61 to 312.88 m depth, resulting in 223 samples. The length of the samples along the drill holes varies from 0.27 to 1.42 m. The samples were collected systematically along the drill holes and packed in individual sampling plastic bags until shipment to Bureau Veritas Commodities Canada Ltd (BVCC) in Santiago, Chile.

The refractory and Rare Earth elements Ba, Be, Ce, Co, Cs, Dy, Er, Eu, Ga, Gd, Hf, Ho, La, Lu, Nb, Nd, Pr, Rb, Sm, Sn, Sr, Ta, Tb, Th, Tm, U, V, W, Y, Yb and Zr were determined by lithium borate fusion with inductively coupled plasma mass spectrometry (ICP-MS), while the trace elements Ag, As, Au, Bi, Cd, Cu, Hg, Mo, Ni, Pb, Sb, Se, Tl and Zn were determined by modified aqua regia digestion (1:1:1 HNO_3:HCl:H_2O) with ICP-MS.

Alkali element mobility and analysis of trace element data

The samples of the metasedimentary rocks were analyzed in order to understand the alkali element mobility in a mineralized hydrothermal system and test the hypothesis that this mobility can be used as a geochemical vector for exploration in the mineralized zones (Kerrich, 1983; Xu, 1999; Eilu et al., 2001; Eilu and Groves, 2001; Heath and Campbell, 2004; Tunussi, 2012).

The modification of a rock's composition is mainly controlled by the migration of fluids, thermal conditions during metamorphism and fluid/rock ratio (Rollinson, 1993). The fluid/rock ratio is generally considerable in orogenic deposits so the hydrothermal alteration in the host rocks results in the addition of significant amounts of CO_2, S, K, H_2O, SiO_2, Na and LILE (Groves et al., 1998). Researchers have been testing hypothesis of alkali element mobility in order to identify and characterize hydrothermal alteration haloes and mineralized zones, as an example, CO_2/(Fe+Mg+Ca) and CO_2/Ca as carbonatation indicators, and (3K+Na)/Al, 3K/Al and Na/Al as sericitization and albitization index (Kishida and Kerrich, 1987; Eilu et al., 1995; Eilu and Groves, 2001; Eilu et al., 2001).

The enrichment of alkalis in the host rocks of gold mineralization have been described in various orogenic belts, and normally these haloes are greater than the visible hydrothermal

alteration, improving the dimensions of the targets for mineral exploration (Kerrich, 1983; Heath and Campbell, 2004).

The mobility of large ion lithophile elements (LILE) and K into solution are predicted to occur during the breakdown of feldspar resulting in alkali enrichment near the mineralization. As the fluids migrate outward from the mineralization, the secondary clays and micas near the ore enrich in LILE and K previously released into solution. The fluid flow is recorded by the disposal of the alkalis around the vein systems. In order to specify a vector to mineralization the outer cooler zones should be enriched in alkalis with greater concentration toward the ore (Heath and Campbell, 2004).

According to Melzer (1999), considerable LILE fractionation between rock and fluid is believed to occur as Rb and Cs may in priority replace K in OH- bearing minerals. The element K is a less sensitive indicator of fluid flow than Rb and Cs. Heath and Campbell (2004) have shown that is possible to map the hydrothermal alteration zones related to gold mineralization beyond the visible alteration zone. This technique allows identifying this halo based on the high ratio of the mobile elements Cs and Rb to the immobile element Th.

To assess the trace element mobility in an altered rock it is necessary to calculate an approximate concentration in that rock prior to alteration. In this work the proper normalization would be in a fresh rock away from the hydrothermal alteration; however, we were unable to find it so we calculated based on upper continental crust normalization (Taylor and McLennan, 1995), which is also suitable because the gold mineralization in Pilar and Três Buracos deposits is hosted in metasedimentary rocks. Consequently, in order to quantify the potential mineralized zones based on alkali element mobility, the Upper Continental Crust normalized ratio $((Cs + Rb)/Th)_{UCC}$ is selected as alteration index for trace elements plot. The mobile elements Cs and Rb are efficient indicators in this specific hydrothermal system due to its tendency of enrichment near mineralized zones and depletion in barren zones.

It is evident that there is a tendency to enrich the alkali elements (Cs, Rb and Ba) near the ore, which corroborates with the petrographic and chemical changes near the mineralized zones **(Figure 15)**.

The mobile and immobile elements association of the mineralized and barren host rock of the Três Buracos deposit is shown in **Figure 16**. From the two drill holes, 160 samples are barren, 36 are subeconomic and 237 are near the ore (HG1 and HG2). The diagrams have shown that there is a clear distribution of the mobile elements in the main gold mineralization and subeconomic samples in comparison with the barren samples. According to Rollingson (1993), these dispersions represent useful indicators for alkali element mobility.

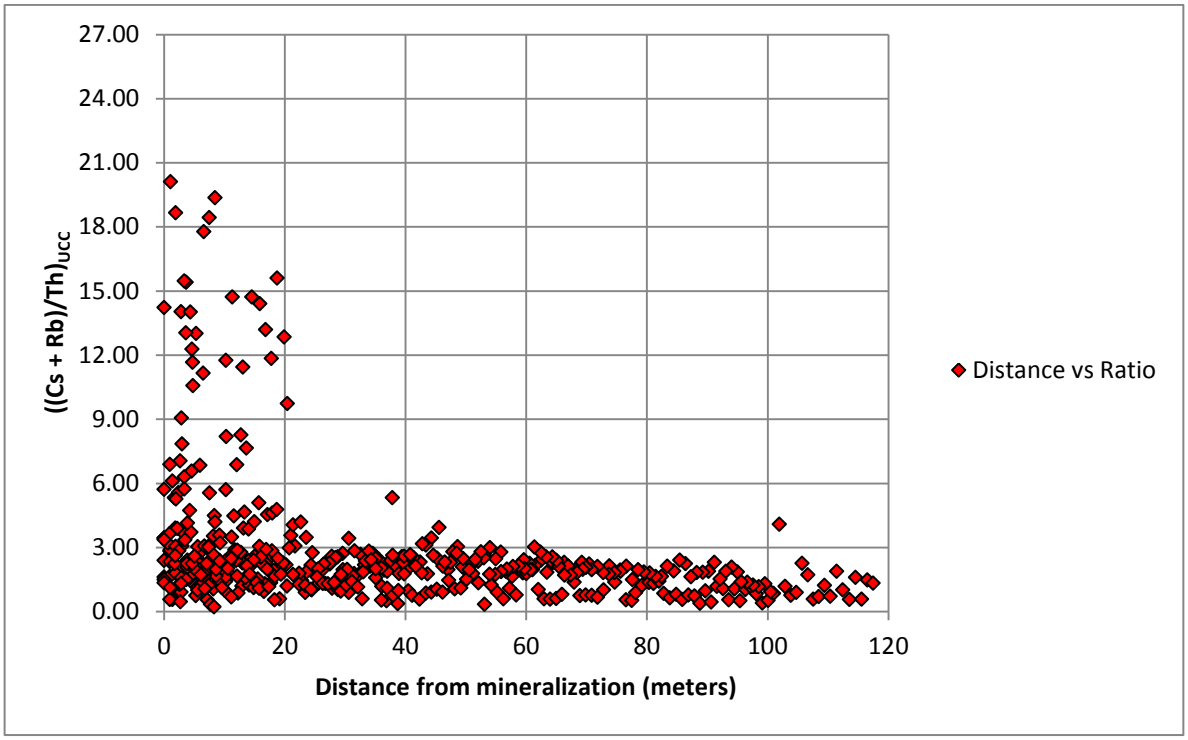

Figure 15. Tendency of alkali element enrichment near mineralization.

The hydrothermal alteration associated with gold mineralization is interpreted as the source of the variation of the alkali element/Th ratio (Heath and Campbell, 2014). The barren samples in the **Figure 16A** have presented slight variation between mobile and immobile elements in the plot. The variation pattern is relatively parallel, showing values similar to the original composition of the rock. This pattern reveals that the modest variation between samples means that they are relatively immobile. The samples are originally equivalent in Rb and Cs when compared to Th, suggesting that hydrothermal alteration has affected barren rocks, however not as much as subeconomic or ore zones.

The samples categorized as subeconomic **(Figure 16B)** vary from alkali enriched to depleted, whether near or far from mineralization. In general, the diagram shows that there is depletion in Cs and Rb, however, enrichment in Ba, when compared to Th. The pattern for samples near the main gold mineralization **(Figure 16C)** is strong mobility for the mobile elements Cs, Rb and Ba, representing strong variation in the alkalis in comparison with barren and subeconomic.

The values for Rb and Cs have a tendency of relatively sub horizontal pattern for barren samples and variable for ore, which corroborate with the mobility characteristic of these elements. The ratio $((Cs + Rb)/Th)_{UCC}$ express the dispersion of the mobile elements with the advantage that Th is an immobile element, reflecting the intensity of the alteration of the ratio

in different hydrothermal conditions. The alkali concentration was divided by the immobile element Th because in reverse of using (Cs + Rb) absolute concentration, high incompatible elements such as U, La and Th probably have had similar variations to the alkali elements in unaltered rocks, this Th normalizing compensates the variation (Heath and Campbell, 2004).

Alkali alteration index

In order to define the alteration index for this study, the 469 samples were considered and the best value to distinguish barren from mineralized samples is 3, where values > 3 are considered enriched in alkali elements and < 3 are considered depleted. The 196 barren and subeconomic samples presented mostly values of $((Cs + Rb)/Th)_{UCC} < 3$, with only 16 examples > 3. The 237 main gold mineralization samples have 148 samples with ratio < 3, however, with a considerable number of 89 samples > 3. The intrusive metagabbro (barren) also was analyzed and returned all 36 values < 3.

Mapping alkali element mobility

The cross section **(Figure 17)** represents the drill holes JOT_002 and JOT_005 plotted with the values for the alteration index $((Cs + Rb)/Th)_{UCC}$. The illustration of the drill holes allows interpreting the hypothesis that the values of the alkali element index increases toward the gold mineralization. The drill holes are deep enough to understand the transition from depletion to enrichment of alkali elements along approximately 300 m. The first half of the drill holes are barren rocks, therefore, resulted in values of $((Cs + Rb)/Th)_{UCC} < 3$. The deepest portions of the drill holes have intercepted two mineralized levels, thus resulting in higher values for the proposed alkali ratio. The metagabbro, which is also barren, has returned values < 3 for the alkali ratio.

7. Discussion and conclusions

Hydrothermal alteration

Previous research (Pulz, 1995) simply described that the mineralization in the Pilar deposit is hosted in a highly strained carbonaceous phyllite and the gold occurs as electrum form associated to arsenopyrite, pyrite, pyrrhotite, sphalerite, galena and chalcopyrite.

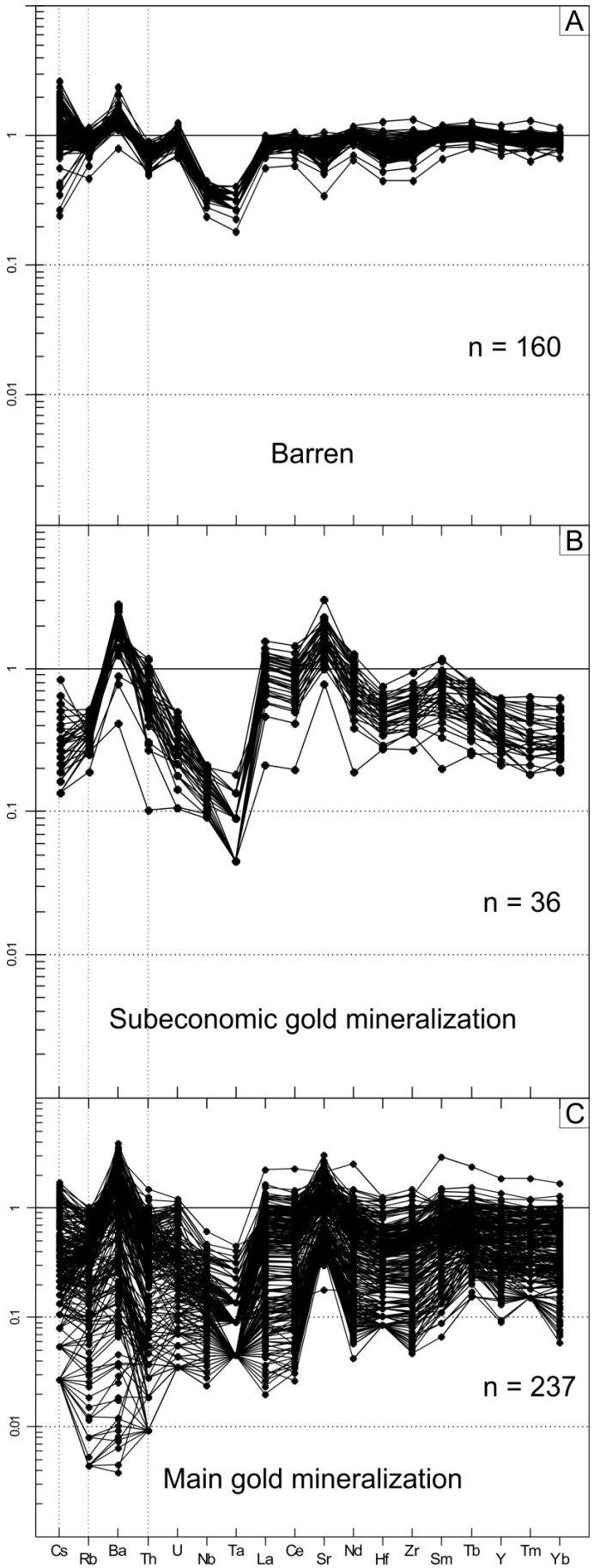

Figure 16. Upper continental crust normalized trace element plots of the Pilar and Três Buracos deposit from drill holes JOT_002 and JOT_005 with varying distance to gold mineralization. (A) Barren samples from distal zone, in the beginning of the drill holes away from the mineralized levels. (B) Subeconomic samples from the isolated samples with considerable gold grade (0.1 to 1 ppm). (C) Ore samples from the main mineralized level (HG1 and HG2) and surroundings. The samples well away from gold mineralization, (A) and (B), are depleted in alkali elements, while the samples near the main gold mineralization (C) are progressively enriched in alkali elements and disturbing plot pattern due to element mobility.

This research has expanded the descriptions and systematically determined the hydrothermal alteration zones from distal to vein based on petrographic and geochemical analysis. This work improves the characterization and positioning of the three main hydrothermal zones firstly identified and described by Jost and Oliveira (1991), which are represented by the mineralized levels HG1, HG2 and HG4.

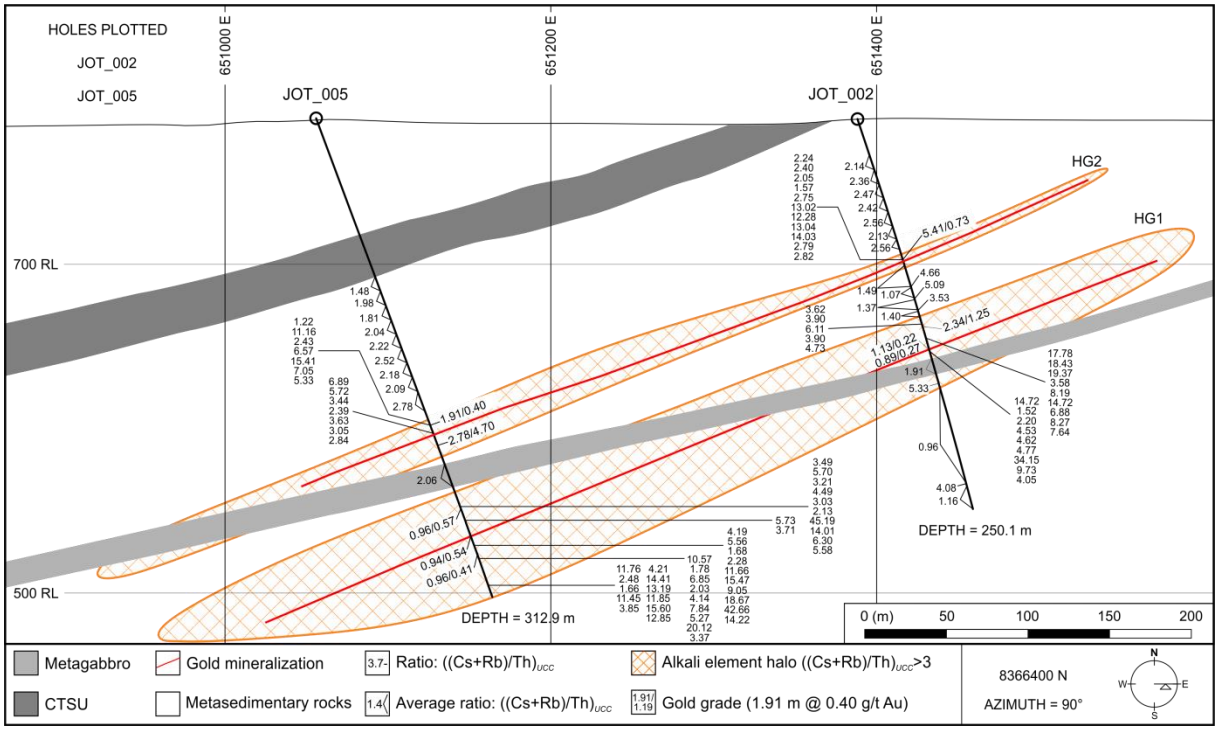

Figure 17. Schematic west-east cross section of drill holes JOT_002 and JOT_005. The $((Cs + Rb)/Th)_{UCC}$ ratio for the samples progressively increases towards the gold mineralization.

Geochemical signature

The alteration index is not a fixed equation and may be changed for different rock types, alteration styles and fluid chemistries. The researchers Heath and Campbell (2004) adopted a value for the alteration index as > 5 using samples enriched in alkali elements for the Archean Yilgarn craton (Australia), while Tunussi (2012) determined a value of 2 for the metabasalts from the Andorinhas greenstone belt (Brazil). This study does not claim to present a universal value for this alteration index. Different rock types have different alteration indices, so the prospects should be investigated to individually determine the best ratio value where applicable.

Fluid flow and alkali element mobility

The alkali element enrichment haloes that surround the mineralized veins intercepted by the drill holes JOT_002 and JOT_005 are interpreted as a result of the fluid that flowed outward the gold lodes and reacted with the wall rock. This setting corroborates with the hypothesis of fluid flow in porous media suggested by Phillips (1991) and reinterpreted in Heath and Campbell (2004). The alkali concentration of the host rock enriches toward gold mineralization, suggesting that the $((Cs + Rb)/Th)_{UCC}$ may be useful when combined with other techniques to explore new gold prospects.

The ratio (Cs + Rb)/Th primitive mantle normalized adopted by Heath and Campbell (2004) to determine mineralized zones based on alkali element mobility enrichment can be used with the same purpose to the Serra do Moinho Formation metasedimentary rocks of the Pilar de Goiás greenstone belt. An upper continental crust normalized (Taylor and McLennan, 1995) ratio of (Cs + Rb)/Th is accurate to differentiate zones of alkali depletion from zones of alkali enrichment in the metasedimentary rocks of the Pilar and Três Buracos deposits. The ratio has shown great discrepancy between mineralized and barren zones, where the mineralized are represented by enrichment in alkali elements and non-mineralized zones are depleted.

The gold mineralization halo associated with the alkali element enrichment is larger than the visible alteration, providing enlarged geochemical vector tracers for gold exploration. The visible alteration halo varies from less than 1 to 5 meters, while the zone of $((Cs + Rb)/Th)_{UCC} > 3$ may reach up to 100 meters. The mineralized zones in the metavolcanosedimentary rocks of the Pilar de Goiás greenstone belt is surrounded by a zone of $((Cs + Rb)/Th)_{UCC}$ that is up to 100 times larger than visible alteration halo. Therefore, alkali-enriched zones are potential exploration targets. Due to the limitations previously explained, we were unable reproduce the method to more drill holes along strike. However, this method is effective to identify geochemical vectors around gold mineralization when applied to sedimentary rocks that have undergone upper greenschist to lower amphibolite facies in a greenstone belt setting.

CAPÍTULO III – CONSIDERAÇÕES FINAIS

Considerações finais

Os dados levantados nessa pesquisa permitiram caracterizar a mineralogia e geoquímica das zonas de alteração hidrotermal associadas aos corpos mineralizados conhecidos do *greenstone belt* Pilar de Goiás e definir vetores prospectivos para a região. Além disso, o mapeamento geológico em escala 1:15.000 efetuado entre os depósitos Pilar e Três Buracos possibilitou compreender a estruturação tectônica do *greenstone belt* Pilar de Goiás e contribuiu para o entendimento da estratigrafia dessa sequencia. Conforme será demonstrado a seguir, foram feitas algumas tentativas de datação da sequência sedimentar e da mineralização.

Contribuições à Estratigrafia do greeenstone belt Pilar de Goiás

A unidade metavulcanossedimentar do *greenstone belt* Pilar de Goiás é denominada Formação Serra do Moinho (Sabóia, 1979; Jost e Oliveira, 1991) e composta por diversas unidades distintas em furos de sondagem, mas difíceis de serem identificadas em campo devido ao estado de fragmentação e intemperismo dos afloramentos. Este trabalho classificou as unidades litológicas da Formação Serra do Moinho tendo como base mais de 100 furos de sondagem do centro-sul e sul da região estudada. Foram identificadas quatro unidades metassedimentares, uma unidade metaultramáfica e um metagabro intrusivo, sendo da base para o topo: xisto feldspático (FSU), biotita – carbonato xisto (BCSU), clorita xisto (CSU), clorita – talco xisto (CTSU), anfibólio xisto (ASU) e metagabro (MGU). A caracterização petrográfica deste trabalho contribuiu para a determinação dos protólitos das unidades da Formação Serra do Moinho, corroborando ou aprimorando descrições anteriores. O protólitos das unidades FSU, BCSU, CSU e ASU foram classificados como sedimentares, CTSU como ultramáfico e MGU ígneo intrusivo. Alguns termos utilizados historicamente pelos geólogos que passaram pela mina de Pilar podem representar produtos de deformação ou alteração hidrotermal, por isso a importância desta reclassificação. Todas as unidades foram detalhadamente descritas nos âmbitos petrográfico e geoquímico, apresentado no Capítulo 2 deste trabalho.

Geoquímica Isotópica

Datação Sm/Nd

A datação pelo método Sm/Nd foi aplicada em rochas da unidade anfibólio xisto (ASU) na tentativa de identificar a idade da mineralização. Para tanto, foram selecionadas amostras posicionadas próximas dos veios mineralizados com granadas. O objetivo era construir isócronas utilizando análises isotópicas Sm-Nd em rocha total e análises isotópicas de granadas metamórficas e hidrotermais, previamente separadas com base morfológica utilizando lupa de mesa.

O método foi aplicado em granadas hidrotermais, granadas metamórficas e rocha total, sendo a preparação e analise executados no Laboratório de Geocronologia da Universidade de Brasília. Porém, a projeção das amostras não foi satisfatória.

Tabela 1. Resultados das amostras coletadas na unidade anfibólio xisto (ASU) analisadas pelo método Sm/Nd.

Amostra	**Sm (ppm)**	**Nd (ppm)**	**$\frac{^{147}Sm}{^{144}Nd}$**	**$^{143}Nd/^{144}Nd$ ± 2SE**	**$\varepsilon_{Nd\,(0)}$**	**Info**
RTB-010A-RT	5.236	28.637	0.1105	0.510970+/-5	-32.54	Rocha total
RTB-010B-RT	2.109	6.629	0.1923	0.512749+/-6	2.16	Rocha total
RTB-010A-H	1.067	0.979	0.6588	0.515439+/-27	54.64	Granadas hidrotermais
RTB-010B-H	0.750	2.970	0.1526	0.512848+/-6	4.11	Granadas hidrotermais
RTB 010B-M	102.385	122.767	0.5041	0.513744+/-31	21.57	Granadas metamórficas

Datação U/Pb

A tentativa de datação da Unidade Metagabro pelo método U/Pb teve intuito de delimitar a idade mínima das rochas sedimentares as quais ele intercepta. Foram coletados aproximadamente 80 quilogramas de amostras desta unidade provenientes de furos de sondagem para separação de zircões, porém foram encontrados apenas 12 grãos após o processo de separação executado no Laboratório de Geocronologia da Universidade de Brasília. Além do baixo número de zircões encontrados, diversos grupos de idades foram identificados **(Figura 18)**, que podem representar zircões herdados, originais da rocha ou eventos mais recentes.

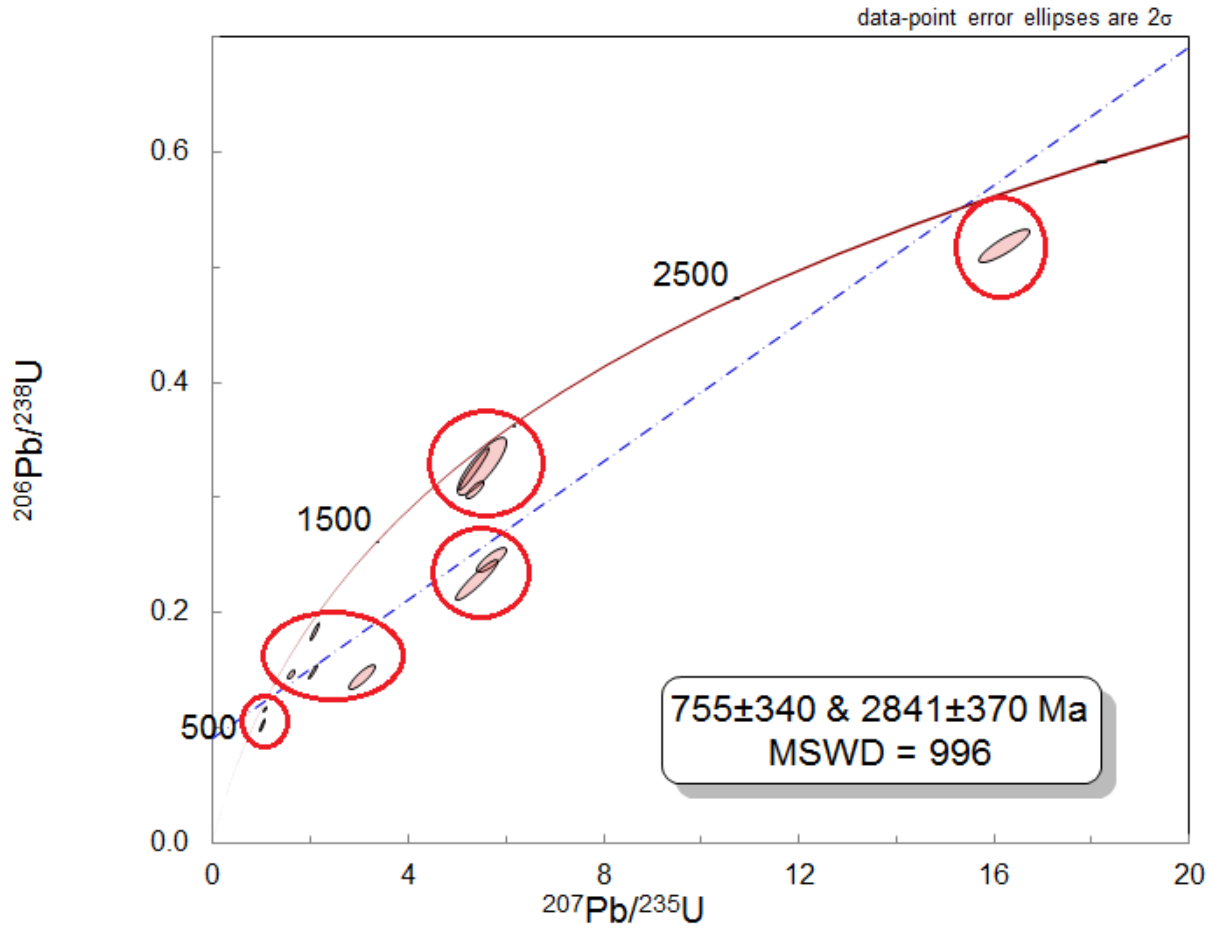

Figura 18. Dados U/Pb dos zircões encontrados no metagabro (MGU) da Formação Serra Geral. Círculos vermelhos indicam grupos de zircões com idades semelhantes.

Mobilidade de elementos álcalis

O estudo sobre mobilidade de álcalis se mostrou muito eficiente para a determinação de vetores geoquímicos nas rochas metassedimentares do *greenstone belt* Pilar de Goiás. O método proposto com sucesso por Heath e Campbell (2004) foi aplicado em rochas máficas do Western Australian Goldfields. Tunussi (2012) também identificou sua eficácia em rochas do *greenstone belt* Andorinhas, porém ainda não havia sido testada em rochas metassedimentares. A razão (Cs + Rb)/Th foi normalizada por *Upper Continental Crust* pelos motivos previamente explicados no Capítulo 2. Os resultados estão dispostos na Figura 17 em forma de seção geológica e sumariza o modelo apresentado dos vetores geoquímicos gerados (Tabela de dados em Anexo). Resta ainda realizar testes em outros tipos de rochas e sistemas minerais.

Trabalhos futuros

O *greenstone belt* Pilar de Goiás tem sido objeto de estudos geológicos nas últimas décadas (descrito no Capítulo 1) por parte tanto da iniciativa privada quanto da iniciativa pública, devido ao seu potencial aurífero e complexidade geológica. Porém, estudos relativos à evolução do *greenstone belt* como um todo, bem como dados geocronológicos confiáveis, ainda são carentes. Áreas como as porções centro e norte da Formação Serra do Moinho, e as outras Formações do *greenstone belt*, ainda necessitam de estudos petrográficos, geoquímicos, geofísicos e de mapeamento para a melhor compreensão da região. O estudo da mobilidade de álcalis aplicado neste trabalho também pode ser testado em todas as áreas remanescentes do *greenstone belt* como um guia para identificação de novos depósitos auríferos.

Referencias bibliográficas

Almeida, F.F.M., Hasui, Y., Brito Neves, B.B., Fuck, R.A., 1981. Brazilian structural provinces: an introduction. Earth-Science Reviews 17(1), 1-29.

Beghelli Junior, L.P., 2012. Charnockitos e ortognaisses da porção centro-oeste do Bloco Arqueano de Goiás: Dados geoquímicos e isotópicos. Dissertação de Mestrado, Instituto de Geociências, Universidade de Brasília, Brasília, pp. 87.

Brito-Neves, B.B., Campos-Neto, M.C., Fuck, R.A., 1999. From Rodinia to Western Gondwana: An approach to the Brasiliano-Pan African cycle and orogenic collage. Episodes 22, 155-199.

Cordeiro, P.F.O., Oliveira, C.G., 2017. The Goiás Massif: implications for a pre-Columbia 2.2-2.0 Ga continent-wide amalgamation cycle in central Brazil. Precambrian Research 298, 403-420.

Corrêa da Costa, P.C., 2003. Petrologia, geoquímica e geocronologia dos diques máficos da região de Crixás-Goiás, porção centro-oeste do Estado de Goiás. Tese de Doutorado, Instituto de Geociências, Universidade de São Paulo, São Paulo, pp. 151.

Danni, J.C.M, Ribeiro, C.C., 1978. Caracterização Estratigráfica da Sequência Vulcanossedimentar de Pilar de Goiás e de Guarinos, Goiás. In: SBG, Congresso Brasileiro de Geologia, Recife, Anais, pp. 582-596.

Danni, J.C.M., Dardenne, M.A., Fuck, R.A., 1981. Geologia da região da Serra da Santa Rita e Sequência Serra de Cantagalo. In: SBG, Simpósio de Geologia do Centro-Oeste, Goiânia, Anais, pp. 265-280.

Danni, J.C.M., Jost, H., Winge, M., Andrade, G.F., 1986. Aspectos da evolução dos terrenos granito-greenstone belt: exemplo da região de Hidrolina, Goiás. In: SBG, Congresso Brasileiro de Geologia, Goiânia, Anais, pp. 570-584.

Dilles, J.H., Einaudi, M.T., 1992. Wall-rock alteration and hydrothermal flow paths about the Ann-Mason porphyry copper deposit, Nevada – a 6-km vertical reconstruction. Economic Geology 87(8), 1963-2001.

de Wit, M.J., 2004. Archean greenstone belts do contain fragments of ophiolites. In: Kusky, T.M. (Ed.), Precambrian Ophiolites and Related Rocks. Developments in Precambrian Geology, vol. 13. Elsevier, Amsterdam, pp. 181–226.

Dubé, B., Gosselin, P., 2007. Greenstone-hosted quartz-carbonate vein deposits. In: Goodfellow, W.D., ed., Mineral Deposits of Canada: A Synthesis of Major Deposit-Types, District Metallogeny, the Evolution of Geological Provinces, and Exploration Methods. Geological Association of Canada, Mineral Deposits Division, Special Publication No. 5, pp. 49-73.

Eilu, P., Groves, D.I., 2001. Primary alteration and geochemical dispersion haloes of Archaean orogenic gold deposits in the Yilgarn Craton: The pre-weathering scenario. Geochemistry Exploration Environment Analysis 1(3), 183-200.

Eilu, P., Groves, D. I., Mikucki, E.J., McNaughton, N.J., Ridley, J.R. 1995. Alteration indices and pathfinder elements in wallrock alteration zones around Archaean lode-gold deposits. In: Passava, J., Kribek, B., Zac, K. (eds.) Mineral Deposits: from their origin to their environmental impacts. Proccedings of the 3rd Bienial SGA Meeting, Prague, 28-31 August 1995. Balkema, Rotterdan, pp. 113-116.

Eilu, P., Mikucki, E.J., Dugdale, A.L., 2001. Alteration zoning and primary geochemical dispersion at the Bronzewing lode-gold deposit, Western Australia. Mineralium Deposita 36, 13-31.

Ellis, D.J., Green, D.H., 1979. An experimental study of the effect of Ca upon garnet-clinopyroxene Fe-Mg exchange equilibria. Contributions to Mineralogy and Petrology 71(1), 13-22.

Ferreira Filho, C.F., Nilson A.A., Naldrett A.J., 1992. The Niquelândia mafic-ultramafic complex, Goiás, Brazil: A contribution to the ophiolite x stratiform controversy based on new geological and structural data. Precambrian Research 59, 125-143.

Ferreira Filho, C.F., Kamo, S.L., Fuck, R.A., Krogh, T.E., Naldrett, A.J., 1994. Zircon and rutile U/Pb geochronology of the Niquelândia layered mafic and ultramafic intrusion, Brazil: constraints for the timing of magmatism and high grade metamorphism. Precambrian Research 68(3-4), 241-255.

Fortes, P.T.F.O., Pimentel, M.M., Santos, R.V., Junges, S., 2003. Sm-Nd study of the Crixás greenstone belt, Brazil: implications for the age of deposition of the upper sedimentary rocks and associated Au mineralization. Journal of South American Earth Sciences 16, 503-512.

Fuck R.A., de Sá E.F.J., Pimentel M.M., Dardenne M.A., Pedrosa Soares, A.C., 1993. As faixas de dobramentos marginais do Cráton do São Francisco: síntese dos conhecimentos. In:

Dominguez, J.M.L., Misi, A. (eds.) O Craton do São Francisco. SBG, Núcleos Bahia e Sergipe, pp. 161-185.

Fuck R.A. 1994. A Faixa Brasília e a compartimentação tectônica na Província Tocantins. In: SBG, Simpósio de Geologia do Centro-Oeste, 4, Brasília, Anais, pp. 184-187.

Furnes, H., Dilek, Y., de Wit, M.J., 2015. Precambrian greenstone sequences represent different ophiolite types. Gondwana Research 27, 649-685.

Giustina, M.E.S.D., Oliveira, C.G., Pimentel, M., Buhn, B., 2009. Neoproterozoic magmatism and high-grade metamorphism in the Goiás Massif: new LA-MC-ICMPS U-Pb and Sm-Nd data and implications for collisional history of the Brasília Belt. Precambrian Research 172, 67-79.

Goldfarb, R.J., Groves, D.I., Gardoll, D., 2001. Orogenic gold and geologic time: A global synthesis. Ore Geology Reviews 18, 1-75.

Goldfarb, R.J., Baker, T., Dubé, B., Groves, D.I., Hart, C.J.R., Robert, F., Gosselin, P., 2005. World distribution, productivity, character, and genesis of gold deposits in metamorphic terranes. In: Hedenquist, J.W., Thompson, J.F.H., Goldfarb, R.J., Richards, J.P., eds., Economic Geology One Hundredth Anniversary Volume: 1905 - 2005: Society of Economic Geologists, pp. 407-450.

Groves, D.J., Goldfarb, R.J., Gebre-Mariam, M., Hagemann, S.G., Robert, F., 1998. Orogenic gold deposits: A proposed classification in the context of their crustal distribution and relationships to other gold deposit types. Ore Geology Reviews, 13, 7-27.

Groves, D.I., Goldfarb, R.J., Robert, F., Hart, C.J.R., 2003. Gold deposits in metamorphic belts: Overview of current understanding, outstanding problems, future research, and exploration significance. Economic Geology 98, 1-29.

Heath, C.J., Campbell, I.H., 2004. A New Geochemical Technique for Gold Exploration: Alkali Element Mobility Associated with Gold Mineralization in the West Australian Goldfields. Economic Geology 99, 313-324.

Hodgson, C.J., 1993. Mesothermal lode-gold deposits. In: Kirkham, R.V., Sinclair, W.D., Thorpe, R.I., Duke, J.M., eds., Mineral Deposits Modelling. Geological Association of Canada, Special Paper 40, pp. 635-678.

Jost, H., Oliveira, A.M., 1991. Stratigraphy of the greenstone belts, Crixás region, Goiás, Central Brazil. Journal of South American Earth Sciences 4, 201 -214.

Jost, H., Oliveira, A.M., Vargas, M.C., 1992. Petrography, geochemistry and structural control of trondhjemitic intrusions in greenstone belts of the Crixás region, Central Brazil. In: SBG, Congresso Brasileiro de Geologia, 37, São Paulo. Anais, pp. 43-44.

Jost, H., Kuyumjian, R.M., Freitas, A.L.S., Costa, A.L.L., Nascimento, C.T.C., Vasconcelos, F.M., Galotti, L., Martins, M.C.A., Carvalho, M.N., Condé, V.C., 1995. Geologia da porção norte do Greenstone Belt de Guarinos, GO. Revista Brasileira de Geociências 25, 51-60.

Jost, H., Fuck, R.A., Dantas, E.L., Rancan, C.C., Rezende, D.B., Santos, E., Portela, J.F., Mattos, L., Chiarini, M.F.N., Oliveira, R.C., Silva, S.E., 2005. Geologia e geocronologia do Complexo Uvá, Bloco Arqueano de Goiás. Revista Brasileira de Geociências 35, 559-572.

Jost, H., Chemale Jr., F., Dussin, I.A., Tassinari, C.C.G., Martins, R., 2010. A U–Pb zircon Paleoproterozoic age for the metasedimentary host rocks and gold mineralization of the Crixás greenstone belt, Goiás, Central Brazil. Ore Geology Reviews 37, 127–139.

Jost, H., Rodrigues, V.G., Carvalho, M.J., Chemale Jr., F., Marques, J.C., 2012. Estratigrafia e geocronologia do greenstone belt de Guarinos, Goiás. Geol. USP, Série científica, São Paulo 12(2), 3-48.

Jost, H., Chemale Jr., F., Fuck, R.A., Dussin, R.A., 2013. Uvá complex, the oldest orthogneisses of the Archean Paleoproterozoic terrane of central Brazil. Journal of South American Earth Sciences 47, 201-212.

Jost, H., Carvalho, M.J., Rodrigues, V.G., Martins, R., 2014. Metalogênese dos greenstone belts de Goiás. In: Silva, M.G., Neto, M.B.R., Jost, H., Kuyumjian, R.M. (Orgs.), Metalogênese das províncias tectônicas brasileiras, Belo Horizonte, CPRM, pp. 141-168.

Junges, S.L., Dantas, E.L., Pimentel, M.M., Laux, J.H., 2002. Idades U-Pb de granitos sin- a tardi-tectônicos do Arco Magmático de Mara Rosa, Goiás. SBG-Núcleo Nordeste, Congresso Brasileiro de Geologia, vol. 41. João Pessoa, Anais, pp. 312.

Junges, S.L., Pimentel, M.M., Dantas, E.L., Laux, J.H., 2003. New ID-TIMS U-Pb ages in the western portion of the Mara Rosa Arc: Two hundred million years of arc building. South American Symposium on the Isotope Geology, vol. 4. Salvador, Short Papers 1, pp. 198-201.

Kerrich, R., 1983. Geochemistry of gold deposits in the Abitibi greenstone belt. Canadian Institute of Mining and Metallurgy Special Paper 27, pp. 75.

Kerrich, R., Feng, R., 1992. Archean geodynamics and the Abitibi- Pontiac collision: Implications for advection of fluids at transpressive collisional boundaries and the origin of giant quartz vein systems. Earth Sciences Reviews 32, 33-60.

Kishida, A., Kerrich, R., 1987. Hydrothermal alteration zoning and gold concentration at the Kerr-Addison Archean Lode Gold Deposit, Kirkland Lake, Ontario. Economic Geology 82, 649-690.

Kuyumjian, R. M., Teixeira, N. A., 1982. Um novo tipo de estrutura em lavas ultramáficas: greenstone belt de Crixás, GO. Revista Brasileira de Geociências 12, 572-577.

Laux, J.H., Pimentel, M.M., Dantas, E.L., Armstrong, R., Junges, S.L., 2005. Two neoproterozoic crustal accretion events in the Brasília Belt, central Brazil. Journal of South American Earth Sciences 18, 183-198.

https://www.leagold.com/_resources/technical-reports/technical-report-pilar-mine-2019.pdf

Melzer, S., 1999. Experimentally determined K-Rb-Cs exchange coefficients between micas, amphiboles and aqueous chlorite solution [abs.]: EOS Supplement 80(17), pp. 361.

Moraes, R., Fuck, R.A., 2000. Ultra-high-temperature metamorphism in Central Brazil: the Barro Alto complex. Journal of Metamorphic Geology 18(4), 345–358.

Phillips, O.M., 1991. Flow and reactions in permeable rocks. Cambridge, Cambridge University Press, pp. 285.

Pimentel, M.M., Heaman, L., Fuck, R.A., 1991. U-Pb zircon and sphene geochronology of late Proterozoic volcanic arc rock units from southwestern Goiás, central Brazil. Journal of South American Earth Sciences 4, 329-339.

Pimentel, M.M., Fuck, R.A., 1992. Neoproterozoic crustal accretion in Central Brazil. Nature 20(4), 375-379.

Pimentel, M.M., Whitehouse, M.J., Vianna, M.G., Fuck, R.A., Machado, N., 1997. The Mara Rosa arc in the Tocantins Province: further evidence for Neoproterozoic crustal accretion in central Brazil. Precambrian Research 81, 299-310.

Pimentel, M.M., Jost, H., Fuck, R.A., Armstrong, R.A., Dantas, E.L., Potrel, A., 2003. Neoproterozoic anatexis of 2.9 Ga old granitoids in the Goiás-Crixás block, Central Brazil: evidence from new SHRIMP U-Pb data and Sm-Nd isotopes. Geologia USP, Série Científica 3, 1-12.

Pimentel, M.M., Jost, H., Fuck, R.A., 2004. O embasamento da Faixa Brasília e o Arco Magmático de Goiás. In: Mantesso-Neto, V., Bartorelli, A., Carneiro, C.D.R., Neves, B.B.B. (Eds.), Geologia do Continente Sul-Americano: evolução da obra de Fernando Fávio Marques de Almeida. Beca Produções Culturais Ltda, São Paulo, pp. 356-368.

Pirajno, F., 2009. Hydrothermal Processes and Mineral Systems. Springer Netherlands 1, pp. 1250.

Piuzana, D., Pimentel, M.M., Fuck, R.A., Armstrong, R., 2003. Neoproterozoic magmatism and high-grade metamorphism in the Brasília Belt, central Brazil: regional implications of SHRIMP U-Pb and Sm-Nd geochronological studies. Precambrian Research 125, 245-273.

Poulsen, K.H., Robert, F., and Dubé, B., 2000. Geological Classification of Canadian Gold Deposits. Geological Survey of Canada, Bulletin 540, pp. 106.

Pulz, G.M., 1995. Modelos prospectivos para ouro em greenstone belts: exemplos dos depósitos Maria Lázara e Ogó, na região de Guarinos e Pilar de Goiás, Goiás. Tese de Doutorado, Instituto de Geociências, Universidade de Brasília, Brasília, pp. 189.

Queiroz, C.L., 2000. Evolução Tectono-Estrutural dos Terrenos Granito-Greenstone Belt de Crixás, Brasil Central. Tese de Doutorado, Instituto de Geociências, Universidade de Brasília, pp. 209.

Queiroz, C.L., Jost, H., Silva, L.C., McNaughton, N.J., 2008. U-Pb SHRIMP and Sm-Nd geochronology of granite-gneiss complexes and implications for the evolution of the central Brazil Archean terrain. Journal of South American Earth Sciences 26, 100-124.

Resende, M.G., Jost, H., 1994. Redefinição da Formação Aimbé, greenstone belt de Guarinos, Goiás, e sua interpretação paleogeográfica e paleotectônica. Boletim de Geociências do Centro-Oeste 17, 49-56.

Resende, L., Jost, H., 1995. Características estratigráficas e petrográficas da sequência metassedimentar do greenstone belt de Pilar de Goiás. SBG Goiânia, Revista Brasileira de Geociências do Centro-Oeste 18 (1/2), 66-83.

Resende, M.G., Jost, H., Osborne, G.A., Mol, A.G., 1998. Stratigraphy of the Goiás and Faina greenstone belts, Central Brazil: a new proposal. Revista Brasileira de Geologia 28, 77-94.

Robert, F., 1995. Quartz-carbonate vein gold. In: Eckstrand, O.R., Sinclair, W.D.T., Thorpe, R.I., eds., Geology of Canadian Mineral Deposit Types. Geological Survey of Canada, Geology of Canada 8, pp. 350-366.

Rodrigues, V.G., 2011. Geologia do depósito aurífero do Caiamar, greenstone belt de Guarinos: um raro depósito associado a albitito sódico. Dissertação de Mestrado, Instituto de Geociências, Universidade de Brasília, Brasília, pp. 79.

Rollingson, H.R. 1993. Using Geochemical Data: evaluation, presentation, interpretation. Longman Scientific & Technical, pp. 352.

Sabóia, L.A., 1979. Os greenstone belts de Crixás e Goiás, GO. SBG, Núcleo Centro-Oeste, Boletim Informativo 9, 44-72.

Seer, H.J., Brod, A.J.A., Fuck, R.A., Pimentel, M.M., Boaventura, G.R., Dardenne, M.A., 2001. Grupo Araxá em sua área tipo: um fragmento de crosta oceânica neoproterozóica na Faixa de Dobramentos Brasília. Revista Brasileira de Geociências 31(3), 385-396.

Strieder, A., Nilson, A.A., 1992. Melange Ofiolítica nos Metassedimentos Araxá de Abadiânia (GO) e Implicações Tectônicas Regionais. Revista Brasileira de Geociências 22(2), 204-215.

Tang, L., Santosh, M., 2017. Neoarchean granite-greenstone belts and related ore mineralization in the North China Craton: An overview. Geoscience Frontiers, 1-18.

Tassinari, C.C.G., Jost, H., Santos, J.C., Nutman, A.P., Bennell, M.R., 2006. Pb and Nd isotope signatures and SHRIMP U-Pb geochronological evidence of paleoproterozoic age for Mina III gold mineralization, Crixás District, Central Brazil. 5th South American Symposium on Isotope Geology, Punta Del Este, Uruguay, Short Papers Volume, pp. 527-529.

Taylor, S.R., McLennan, S.M., 1995. The geochemical evolution of the continental crust. Reviews of Geophysics 33(2), 241-265.

Teixeira, A.S., 1981. Geologia da região de Goiás-Faina. SBG, Simpósio Geologia Centro-Oeste, Atas, Goiânia, pp. 344-360.

Teixeira, N.A., Saboia, L.A., Ferreira, M.C.B., Teixeira, A.S., Castro, J.H.G., 1981. Estruturas e texturas das lavas ultrabásicas e básicas do greenstone belt de Crixás, Goiás, Brasil. SBG, Núcleo do Centro-Oeste, Boletim Informativo 10, 33-87.

Tunussi, C., 2012. Integração de dados multifonte para caracterização das zonas de alteração hidrotermal associadas às mineralizações de ouro no greenstone belt andorinhas, província mineral de carajás. Dissertação de Mestrado, Instituto de Geociências, Universidade de Brasília, Brasília, pp. 145.

Valeriano C.M., Dardenne M.A., Fonseca M.A., Simões L.S.A., Seer H.J. 2004. A evolução tectônica da Faixa Brasília. In: Mantesso-Neto, V., Bartorelli, A., Carneiro, C.D.R., Brito Neves, B.B. (eds). Geologia do Continente Sul-Americano: evolução e obra de Fernando Flávio Marques de Almeida. Beca, São Paulo, pp. 575-593.

Van Kranendonk, M.J., 2007. A review of the evidence for putative paleoarchean life in the Pilbara Craton, Western Australia. In: Earth's Oldest Rocks, pp. 855-877.

Xu, Y., 1999. The stable isotope and trace element geochemistry of the Victory gold deposit, Western Australia. Ph.D. thesis, Canberra, ACT, The Australian National University, pp. 145.

Zhu, Y., Na, F., Tan, J., 2011. Geochemistry of hydrothermal gold deposits: A review. Geoscience Frontiers 2 (3), 367-374.

Anexo A

DHID	DATUM_UTM	X	Y	Z	AZIMUTH	DIP	DEPTH (m)
JD_503	SAD 69 - ZONE 22S	649637.21	8368094.82	783.93	71.58	-70.00	545.38
JD_504	SAD 69 - ZONE 22S	650650.77	8367500.40	883.39	69.60	-71.09	353.42
JD_507	SAD 69 - ZONE 22S	650846.21	8367653.78	897.80	70.66	-70.42	244.62
JD_514	SAD 69 - ZONE 22S	650987.32	8367647.85	846.86	70.29	-71.25	184.63
JD_515	SAD 69 - ZONE 22S	650125.99	8367645.98	803.69	69.33	-71.47	470.43
JD_519	SAD 69 - ZONE 22S	650801.36	8367901.72	841.75	69.97	-70.97	196.66
JD_520	SAD 69 - ZONE 22S	650898.60	8367790.27	853.68	71.50	-70.83	162.63
JD_523	SAD 69 - ZONE 22S	650468.62	8367958.23	881.54	70.87	-71.02	299.53
JD_526	SAD 69 - ZONE 22S	650783.13	8367996.51	823.86	70.13	-70.22	130.13
JD_527	SAD 69 - ZONE 22S	650390.95	8368342.08	829.98	69.29	-71.23	181.85
JD_528	SAD 69 - ZONE 22S	650644.92	8367934.33	869.45	70.71	-70.00	228.22
JD_529	SAD 69 - ZONE 22S	650696.77	8368051.82	823.99	71.56	-71.07	139.30
JD_531	SAD 69 - ZONE 22S	650536.01	8368103.70	850.29	71.69	-71.00	212.03
JD_533	SAD 69 - ZONE 22S	650449.16	8368221.32	835.35	63.81	-70.56	167.45
JD_535	SAD 69 - ZONE 22S	650260.87	8368525.27	858.01	68.70	-69.41	226.69
JD_536	SAD 69 - ZONE 22S	650265.62	8368439.21	850.99	69.91	-70.51	244.61
JD_537	SAD 69 - ZONE 22S	650227.28	8368670.48	864.20	71.67	-70.69	229.63
JD_539	SAD 69 - ZONE 22S	649173.31	8368544.41	751.42	69.94	-70.00	635.43
JD_592	SAD 69 - ZONE 22S	649765.88	8368348.42	767.25	0.48	-70.68	259.00
JOT_046	SAD 69 - ZONE 22S	649748.94	8368905.00	804.75	70.00	-70.00	161.88
JOT_047	SAD 69 - ZONE 22S	649499.38	8368765.50	754.18	70.00	-70.00	147.97
JOT_048	SAD 69 - ZONE 22S	649761.25	8368947.50	799.49	70.00	-70.00	208.77
JOT_049	SAD 69 - ZONE 22S	649428.56	8368731.50	758.01	70.00	-70.00	247.62
JOT_050	SAD 69 - ZONE 22S	649541.63	8368726.50	751.86	70.00	-70.00	180.94
JOT_051	SAD 69 - ZONE 22S	649485.31	8368818.50	751.81	70.00	-70.00	211.71
JOT_052	SAD 69 - ZONE 22S	649653.06	8368847.50	795.35	70.00	-70.00	239.82
JOT_053	SAD 69 - ZONE 22S	649771.00	8368859.50	816.51	70.00	-70.00	229.31
JOT_054	SAD 69 - ZONE 22S	649865.63	8368734.00	821.54	70.00	-70.00	115.58
JOT_055	SAD 69 - ZONE 22S	649851.63	8368845.50	831.48	70.00	-70.00	114.31
JOT_056	SAD 69 - ZONE 22S	649922.56	8368946.00	837.71	70.00	-70.00	67.99
JOT_057	SAD 69 - ZONE 22S	649809.69	8368799.50	824.85	0.00	-90.00	146.31
JOT_058	SAD 69 - ZONE 22S	649596.56	8368804.00	765.63	70.00	-70.00	114.17
JOT_059	SAD 69 - ZONE 22S	649857.88	8368937.00	827.99	70.00	-70.00	94.55
JOT_060	SAD 69 - ZONE 22S	649888.06	8368875.50	837.76	70.00	-70.00	106.79
JOT_071	SAD 69 - ZONE 22S	649744.38	8368764.50	811.17	70.00	-70.00	133.23
JOT_072	SAD 69 - ZONE 22S	649728.19	8368724.50	804.31	70.00	-70.00	137.56
JOT_073	SAD 69 - ZONE 22S	649857.88	8368937.00	827.99	0.00	-90.00	57.96
JOT_074	SAD 69 - ZONE 22S	649827.94	8368882.50	827.62	70.00	-70.00	118.73
JOT_075	SAD 69 - ZONE 22S	649952.75	8368801.50	844.65	70.00	-70.00	121.39
JOT_076	SAD 69 - ZONE 22S	649729.00	8368832.00	807.34	70.00	-70.00	123.17
JOT_077	SAD 69 - ZONE 22S	649923.56	8368672.00	815.30	70.00	-70.00	110.97

JOT_078	SAD 69 - ZONE 22S	649690.25	8368644.50	772.00	70.00	-70.00	143.99
JOT_079	SAD 69 - ZONE 22S	649929.13	8368905.00	848.00	70.00	-70.00	94.88
JOT_080	SAD 69 - ZONE 22S	649717.19	8368876.00	809.00	70.00	-70.00	112.18
JOT_081	SAD 69 - ZONE 22S	649694.88	8368816.00	809.32	70.00	-70.00	128.60
JOT_082	SAD 69 - ZONE 22S	649995.19	8368936.50	851.00	70.00	-70.00	75.28
JOT_083	SAD 69 - ZONE 22S	649961.13	8368865.00	859.32	70.00	-70.00	106.28
JOT_084	SAD 69 - ZONE 22S	649922.94	8368836.50	846.64	70.00	-70.00	115.92
JOT_085	SAD 69 - ZONE 22S	649885.94	8368803.50	839.57	70.00	-70.00	120.25
JOT_087	SAD 69 - ZONE 22S	649963.19	8368772.50	838.63	70.00	-70.00	140.69
JOT_090	SAD 69 - ZONE 22S	650002.19	8368705.50	827.12	70.00	-70.00	95.16
JOT_091	SAD 69 - ZONE 22S	650073.63	8368632.50	839.41	70.00	-70.00	108.63
JOT_092	SAD 69 - ZONE 22S	650056.56	8368485.50	826.19	70.00	-70.00	137.02
JOT_093	SAD 69 - ZONE 22S	649851.38	8368599.00	792.11	70.00	-70.00	138.34
JOT_094	SAD 69 - ZONE 22S	650160.69	8368683.50	852.70	60.00	-70.00	67.87
JOT_095	SAD 69 - ZONE 22S	650098.38	8368771.50	854.01	70.00	-70.00	83.62
JOT_097	SAD 69 - ZONE 22S	650135.69	8368437.50	830.31	70.00	-70.00	134.02
JOT_098	SAD 69 - ZONE 22S	649988.06	8368571.00	826.21	60.00	-70.00	130.60
JOT_099	SAD 69 - ZONE 22S	649903.69	8368520.00	805.45	70.00	-70.00	161.12
JOT_100	SAD 69 - ZONE 22S	649681.00	8368969.00	776.48	70.00	-70.00	63.04
JOT_121	SAD 69 - ZONE 22S	650745.24	8367591.58	902.90	70.00	-68.69	335.43
JOT_123	SAD 69 - ZONE 22S	650557.44	8367836.50	892.59	70.00	-67.87	293.40
JOT_125	SAD 69 - ZONE 22S	650395.87	8368081.13	870.50	70.00	-69.27	282.97
JOT_127	SAD 69 - ZONE 22S	650353.87	8368229.42	860.01	70.00	-70.45	266.42
JOT_129	SAD 69 - ZONE 22S	650193.61	8368348.63	847.16	70.00	-69.29	338.43
JOT_131	SAD 69 - ZONE 22S	650917.02	8367519.05	899.22	70.00	-69.12	245.43
JOT_133	SAD 69 - ZONE 22S	650751.29	8367757.85	901.20	70.00	-68.30	500.33
JOT_135	SAD 69 - ZONE 22S	650569.99	8368007.64	864.07	70.00	-68.66	227.34
JOT_137	SAD 69 - ZONE 22S	650135.62	8368560.63	851.06	70.00	-71.10	278.43
JOT_147	SAD 69 - ZONE 22S	650245.00	8368736.00	862.60	60.00	-70.00	70.85
TB_001	SAD 69 - ZONE 22S	650051.50	8368847.25	864.28	73.45	-74.97	239.20
TB_002	SAD 69 - ZONE 22S	649639.18	8368756.67	773.76	65.95	-74.38	351.84
TB_003	SAD 69 - ZONE 22S	649797.15	8368689.78	803.47	98.29	-75.59	362.16
TB_004	SAD 69 - ZONE 22S	650005.85	8368450.00	813.02	66.40	-82.69	313.75
TB_005	SAD 69 - ZONE 22S	649640.75	8368671.46	765.44	64.77	-65.11	349.18
TB_006	SAD 69 - ZONE 22S	649563.06	8368893.90	759.22	73.86	-75.65	320.22
TB_007	SAD 69 - ZONE 22S	649695.28	8368991.06	776.72	0.83	-69.88	272.40
TB_008	SAD 69 - ZONE 22S	650010.79	8368642.79	827.34	70.55	-75.51	301.56
TB_009	SAD 69 - ZONE 22S	649668.90	8368893.79	794.16	1.68	-75.09	311.43
TB_010	SAD 69 - ZONE 22S	649601.32	8368581.81	760.19	0.79	-74.60	448.67
TB_011	SAD 69 - ZONE 22S	649837.50	8368520.37	790.19	331.85	-70.34	403.27
TB_012	SAD 69 - ZONE 22S	650085.39	8368687.94	839.66	59.28	-72.95	280.11
TB_013	SAD 69 - ZONE 22S	649869.03	8368497.50	792.05	99.43	-79.49	359.29
TB_014	SAD 69 - ZONE 22S	650026.44	8368880.43	861.20	70.06	-71.18	255.69
TB_015	SAD 69 - ZONE 22S	649482.07	8368654.20	755.23	71.74	-77.52	440.50
TB_016	SAD 69 - ZONE 22S	649901.15	8368921.41	835.55	72.49	-74.63	118.44

TB_017	SAD 69 - ZONE 22S	649585.37	8369186.14	785.97	66.43	-80.82	307.55
TB_018	SAD 69 - ZONE 22S	649648.81	8368509.62	761.79	69.05	-75.05	444.15
TB_019	SAD 69 - ZONE 22S	649981.07	8368251.64	795.34	74.02	-79.36	372.61

Anexo B

Sample	From	To	Unit	Cs (ppm)	Rb (ppm)	Th (ppm)	((Cs + Rb)/Th) UCC
				Drill hole JOT_002			
2979	23.14	24.36	CSU	4	81	6.6	2.23
2981	25.08	26.08	CSU	5.2	105.4	8.3	2.30
2982	26.08	27.04	CSU	3.6	94.6	7.8	1.96
2983	27.04	28.01	CSU	3.4	87.4	7.9	1.80
2984	28.01	28.97	CSU	4.6	94.7	7.4	2.30
2985	28.97	29.92	CSU	4.8	91.5	7.9	2.16
2986	29.92	30.88	CSU	5.1	91.7	7.7	2.29
2987	30.88	31.82	CSU	4.1	83.4	8.2	1.84
2988	31.82	32.81	CSU	5	98	7.5	2.41
2989	32.81	33.73	CSU	3.5	86	6.6	2.16
2990	33.73	34.71	CSU	3.9	106.7	7.5	2.26
2991	34.71	35.67	CSU	3.9	109.3	7.1	2.42
2992	35.67	36.64	CSU	3.5	98.4	7.3	2.11
2993	36.64	37.6	CSU	2.9	84.4	7.9	1.65
2994	37.6	38.5	CSU	4.3	88.2	8.5	1.87
2995	38.5	39.38	CSU	5.7	97	6.9	2.78
2996	39.38	40.32	CSU	6.8	85.2	8.1	2.48
2998	40.32	41.28	CSU	7.2	96.5	7.3	2.99
2999	41.28	42.25	CSU	6	98.4	7.5	2.65
3000	42.25	43.19	CSU	5.2	97	7.8	2.35
3001	43.19	44.05	CSU	3.3	93.9	8.2	1.79
3002	44.05	44.85	CSU	3.6	100.7	8.4	1.88
3003	44.85	45.65	CSU	3.7	97.1	7.5	2.09
3004	45.65	46.47	CSU	6.1	111.7	7	3.04
3005	46.47	47.26	CSU	6.8	110.7	8	2.81
3006	47.26	48.12	CSU	3.8	105.2	8.5	1.95
3007	48.12	49.07	CSU	3.7	99.4	7.5	2.12
3008	49.07	50.02	CSU	6.6	102.2	8.5	2.50
3009	50.02	50.91	CSU	8.9	106.6	7.5	3.44
3010	50.91	51.49	CSU	7.7	109.9	7.7	3.11
3011	51.49	51.86	CSU	4.8	94.9	5.5	3.17
3012	51.86	52.96	CSU	4	100.2	7.1	2.32
3013	52.96	53.95	CSU	4.8	101.2	7.1	2.54
3014	53.95	54.9	CSU	3.4	99	7.7	1.99
3015	54.9	55.87	CSU	4.7	94.5	6.7	2.57
3016	55.87	56.83	CSU	3.2	99.9	7.2	2.09

Sample	From	To	Unit	Cs (ppm)	Rb (ppm)	Th (ppm)	((Cs + Rb)/Th) UCC
3017	56.83	57.79	CSU	4.3	110.8	7.5	2.40
3019	57.79	58.73	CSU	4	88.5	7.9	1.95
3020	58.73	59.71	CSU	4.1	94.5	6.6	2.44
3021	59.71	60.75	CSU	5.1	100.6	6.8	2.72
3022	60.75	61.75	CSU	5	94.6	7.6	2.33
3023	61.75	62.77	CSU	5.2	101.6	7	2.68
3024	62.77	63.72	CSU	7.1	111.1	8.1	2.84
3025	63.72	64.7	CSU	7.3	96.2	6.4	3.43
3026	64.7	65.58	CSU	7.5	99.1	8.3	2.72
3027	65.58	66.49	CSU	5.8	97.9	7.6	2.56
3028	66.49	66.82	CSU	5	120.7	7.8	2.59
3029	66.82	67.52	CSU	4.8	100	8	2.24
3030	67.52	68.18	CSU	4.4	101.2	7.6	2.27
3031	68.18	69.12	CSU	3.5	96.9	7.9	1.94
3032	69.12	69.98	CSU	3.8	96.5	8.1	1.95
3033	69.98	70.77	CSU	3.5	95.4	7	2.16
3034	70.77	71.48	CSU	3.4	90.9	7.9	1.84
3035	71.48	72.13	CSU	3.2	89.5	9.7	1.45
3036	72.13	73.3	CSU	3.1	88.8	8.1	1.71
3037	73.3	74.07	CSU	9.8	110.7	7.8	3.56
3038	74.07	75.1	CSU	5	102.9	8.5	2.18
3040	75.1	76.09	CSU	3.6	88	7.1	2.06
3041	76.09	77.05	CSU	3	98.2	7.5	1.94
3042	77.05	77.5	CSU	3.2	99.4	6.1	2.46
3043	77.5	78.49	CSU	4.3	107.4	7.8	2.27
3044	78.49	79.31	CSU	4.6	88.5	5.4	3.05
3045	79.31	80.31	CSU	5.1	105.2	7.3	2.59
3046	80.31	81.32	CSU	5	106.1	7.9	2.38
3047	81.32	81.87	CSU	3.5	130.3	8.1	2.27
3048	81.87	83.03	CSU	2.9	107.3	5.7	2.67
3049	83.03	84.05	CSU	3.2	128.3	6.6	2.68
3050	84.05	85.15	BCSU	3.8	105.1	7.4	0.89
3051	85.15	86.34	BCSU	4.1	93.7	6.7	0.89
3052	86.34	87.49	BCSU	4.3	98.1	8.2	1.01
3053	87.49	88.37	BCSU	3.1	94	9.1	1.03
3054	88.37	89.01	BCSU	4.8	99.8	6.5	1.09
3055	89.01	89.71	BCSU	4.7	77.7	1.2	1.31
3057	89.71	90.71	BCSU	4.3	88.9	1.3	1.33
3058	90.71	91.49	BCSU	4.1	89.4	1.2	1.79
3059	91.49	92.45	BCSU	5.8	114.8	1.5	1.79
3061	92.45	93.34	BCSU	2.4	55.8	3.4	1.96
3062	93.34	94.32	BCSU	2.5	49	3.2	0.85
3063	94.32	95.12	FSU	1.8	48.8	4.8	1.06
3064	95.12	96.12	FSU	2.6	49.5	3.2	1.10
3065	96.12	97	FSU	1.6	42.2	9.8	1.22

Sample	From	To	Unit	Cs (ppm)	Rb (ppm)	Th (ppm)	((Cs + Rb)/Th) UCC
3066	97	97.94	FSU	1.4	37.6	6.6	1.31
3067	97.94	98.99	FSU	2.1	52.7	3.8	1.35
3068	98.99	99.98	FSU	1.2	40.3	4.5	1.41
3069	99.98	100.69	FSU	0.8	35.5	4.1	1.51
3070	100.69	101.6	FSU	1.8	55.7	4.7	2.24
3071	101.6	102.29	FSU	1.3	51.7	12.8	2.24
3072	102.29	103.28	FSU	1	54.2	6.5	2.40
3073	103.28	104.23	FSU	1.3	49.9	3.9	2.05
3074	104.23	105.18	FSU	1.1	40.7	5.8	1.57
3075	105.18	106.15	FSU	1.4	48	4.1	2.75
3076	106.15	107.09	FSU	2.8	69.9	4.8	13.02
3077	107.09	108.01	FSU	1.4	49.1	5.9	12.28
3078	108.01	108.44	FSU	3.4	64.9	2.6	13.04
3079	108.44	109.27	FSU	0.5	26.5	2.7	14.03
3080	109.27	110	FSU	0.4	34.6	3.5	2.79
3082	110	110.77	FSU	1	49.3	4.5	2.82
3083	110.77	111.71	FSU	0.9	43.6	6	3.62
3084	111.71	112.55	FSU	0.4	32.8	6.4	1.27
3085	112.55	113.21	FSU	0.5	34.2	7.5	3.90
3086	113.21	114.18	FSU	1.6	50.2	5.6	1.65
3087	114.18	115.16	FSU	0.7	43.7	4.1	1.49
3088	115.16	116.24	FSU	0.6	48.4	1.1	3.45
3089	116.24	117.41	FSU	1	54.9	3.1	3.20
3090	117.41	118.6	FSU	1.5	62.7	5.4	6.11
3091	118.6	119.74	FSU	0.3	37.5	4.7	3.90
3092	119.74	120.7	FSU	0.6	40.5	7	3.07
3093	120.7	121.69	FSU	1.4	50.2	5.1	3.36
3094	121.69	122.71	FSU	1	46.9	4.3	2.41
3095	122.71	123.7	FSU	2.8	97.9	4	4.73
3096	123.7	124.69	FSU	1.6	70.8	4.7	1.75
3097	124.69	125.61	FSU	0.5	45.3	4.1	3.04
3098	125.61	126.53	FSU	0.8	55.4	8.9	1.59
3099	126.53	127.48	FSU	0.9	51.5	4	1.19
3100	127.48	128.31	BCSU	2.5	72.4	3.1	0.58
3101	128.31	128.99	BCSU	0.6	30.7	3.1	0.86
3103	128.99	129.93	BCSU	1	35.2	1.3	0.91
3104	129.93	130.88	BCSU	1.1	39	3.4	1.05
3105	130.88	131.85	BCSU	0.8	31	2.9	0.92
3106	131.85	132.55	BCSU	0.7	38.3	1.4	1.46
3107	132.55	133.22	BCSU	1	73.3	2.7	1.94
3108	133.22	133.93	BCSU	2.9	108	2.5	0.55
3109	133.93	134.73	BCSU	2.8	109.2	3.9	0.53
3110	134.73	135.51	BCSU	1.2	46.2	2.1	0.88
3111	135.51	136.03	BCSU	1.5	46.8	2.1	17.78
3112	136.03	136.43	BCSU	0.4	10.4	0.7	18.43

Sample	From	To	Unit	Cs (ppm)	Rb (ppm)	Th (ppm)	((Cs + Rb)/Th) UCC
3113	136.43	136.82	BCSU	0.2	6.3	0.2	19.37
3114	136.82	137.28	BCSU	1.5	44.4	3.9	3.58
3115	137.28	138.14	BCSU	0.8	20.5	1.1	8.19
3116	138.14	139.14	BCSU	0.8	22.8	0.2	14.72
3117	139.14	140.03	BCSU	1.8	44.6	0.4	6.88
3118	140.03	140.99	BCSU	1.4	35.5	0.3	8.27
3119	140.99	141.74	BCSU	0.5	21.1	0.8	7.64
3120	141.74	142.87	BCSU	1.1	49.1	0.8	14.72
3121	142.87	143.85	BCSU	1.5	65.9	0.6	1.52
3122	143.85	144.63	BCSU	0.8	43.6	0.8	2.20
3124	144.63	145.29	BCSU	0.6	41.6	0.6	4.53
3125	145.29	146.18	BCSU	0.3	18.8	0.3	4.62
3126	146.18	147.09	BCSU	0.8	47.7	0.4	4.77
3127	147.09	148.08	BCSU	0.1	9.5	0.7	34.15
3128	148.08	148.91	BCSU	0.1	7.5	0.4	9.73
3129	148.91	149.68	BCSU	0.5	14.7	0.5	4.05
3130	149.68	150.5	BCSU	0.7	16.3	0.6	0.60
3131	150.5	151.22	BCSU	0.5	10.9	0.4	2.83
3132	151.22	152.06	BCSU	0.9	19.4	0.1	0.51
3133	152.06	152.97	BCSU	0.8	16	0.3	5.33
3134	152.97	153.92	BCSU	0.8	15.1	0.7	0.38
3146	164.07	165.41	BCSU	0.1	1.3	0.5	1.31
3147	165.41	166.49	BCSU	0.8	15	1	1.16
3148	166.49	167.6	BCSU	0.2	4.7	0.5	1.79
3149	167.6	168.63	BCSU	0.7	14.6	2.2	0.56
3150	168.63	169.43	BCSU	0.5	9	3.4	1.05
3151	169.43	170.38	BCSU	0.4	9.5	0.3	1.79
3152	170.38	171.27	BCSU	0.6	12.9	6	0.99
3153	171.27	172.17	BCSU	4.9	41.2	5.5	1.70
3154	172.17	173.03	BCSU	2.2	24.8	6.4	2.40
3155	173.03	173.67	BCSU	3.8	56.3	15.9	1.20
3156	173.67	174.88	BCSU	0.9	46.4	10.2	4.66
3158	174.88	175.95	BCSU	0.8	40.1	6	1.25
3159	175.95	176.83	BCSU	0.8	42.9	6	1.13
3160	176.83	177.75	BCSU	0.9	43.2	5.4	1.42
3161	177.75	178.73	BCSU	0.6	30.7	4.3	0.95
3162	178.73	179.74	BCSU	1.3	52	4.9	0.59
3168	183.61	184.67	FSU	1.3	40	4.5	2.23
3169	184.67	185.65	FSU	0.4	25.1	9.1	1.58
3170	185.65	186.76	FSU	1.6	49.1	6	0.86
3171	186.76	187.76	FSU	2.1	41.9	8.6	0.69
3172	187.76	188.78	FSU	1	38.5	9	1.41
3173	188.78	189.81	FSU	1	41.7	5.2	1.43
3174	189.81	190.9	FSU	1	50.8	8.4	3.53
3175	190.9	192.05	FSU	1.8	58.4	4.8	2.02

Sample	From	To	Unit	Cs (ppm)	Rb (ppm)	Th (ppm)	((Cs + Rb)/Th) UCC
3176	192.05	192.61	BCSU	1.1	38.1	3.1	1.25
3177	192.61	193.59	BCSU	0.8	26.6	2	0.74
3178	193.59	194.57	FSU	1.4	58.1	7.7	1.61
3179	194.57	195.51	FSU	0.7	43.1	8.8	1.35
3180	195.51	196.55	FSU	0.5	39.5	7.9	0.34
3181	196.55	197.52	FSU	0.5	38.4	7.4	1.24
3182	197.52	198.52	FSU	0.6	45	6.6	0.89
3183	198.52	199.52	FSU	2	89.9	5.6	0.60
3184	199.52	200.52	FSU	1.4	76.1	7	1.09
3185	200.52	201.48	FSU	0.6	51.4	7.8	0.78
3187	201.48	202.4	FSU	0.6	61.2	8.7	1.81
3188	202.4	203.42	FSU	0.5	49.7	7.3	1.03
3189	203.42	204.36	FSU	0.6	43.8	7.7	0.60
3190	204.36	205.39	FSU	1	55.6	6.9	0.58
3191	205.39	206.33	FSU	1.5	56.3	3.7	0.61
3192	206.33	207.26	FSU	1.3	53.3	5.3	0.80
3193	207.26	208.17	BCSU	1.5	42	3.4	2.14
3194	208.17	209.12	BCSU	2	41	13.4	1.37
3195	209.12	210.06	BCSU	1.4	35.6	11	0.75
3196	210.06	210.69	BCSU	1.9	49.9	9.1	0.78
3202	215.35	216.36	FSU	2.1	45.9	12.6	0.64
3203	216.36	217.41	FSU	1.9	37.6	8.6	0.80
3204	217.41	218.43	FSU	1.4	33.9	10.1	0.56
3205	218.43	219.45	FSU	1.4	42.3	8.3	0.78
3206	219.45	220.46	FSU	1.1	37	7.4	0.73
3208	220.46	221.34	FSU	0.8	30	11.1	0.38
3209	221.34	222.24	FSU	1.1	40.4	5.9	0.97
3210	222.24	223.21	FSU	0.7	38	10.9	0.44
3211	223.21	224.19	FSU	1.2	37.6	4.8	1.18
3212	224.19	225.16	FSU	1.2	57.3	7	1.07
3213	225.16	226.12	FSU	0.5	31.4	7	0.55
3214	226.12	227.07	FSU	1.1	47.3	6	1.06
3215	227.07	227.99	FSU	0.7	37.8	9.5	0.50
3216	227.99	228.9	FSU	0.9	37.8	5	1.03
3217	228.9	229.72	FSU	0.7	27.9	3.3	1.17
3218	229.72	230.69	FSU	1.5	48.9	8.6	0.84
3219	230.69	231.69	FSU	0.5	21.2	7.2	0.40
3220	231.69	232.65	FSU	1.2	45.6	12.3	0.52
3221	232.65	233.55	FSU	1.1	40.2	6.7	0.85
3222	233.55	234.53	FSU	1	29	1.1	4.08
3223	234.53	235.49	FSU	1.2	50.7	5.8	1.19
3224	235.49	236.41	FSU	0.9	42.7	7.3	0.77
3225	236.41	237.34	FSU	0.9	42.1	6.2	0.89
3226	237.34	238.29	FSU	1	50.9	2.9	2.26
3227	238.29	239.21	FSU	0.7	45.7	3.2	1.73

Sample	From	To	Unit	Cs (ppm)	Rb (ppm)	Th (ppm)	((Cs + Rb)/Th) UCC
3229	239.21	240.12	FSU	0.6	32.9	7.1	0.58
3230	240.12	241.02	FSU	0.5	30.3	5.3	0.70
3231	241.02	242.01	FSU	1.1	49.5	5.4	1.22
3232	242.01	242.94	FSU	0.7	36.9	6.6	0.71
3233	242.94	244.01	FSU	1.7	54.2	4.3	1.88
3234	244.01	245	FSU	0.8	40	5.1	1.01
3235	245	246.15	FSU	0.6	34.9	7.6	0.57
3236	246.15	247.16	FSU	1.9	57.7	5.5	1.60
3237	247.16	248.14	FSU	1.1	43.2	10.4	0.58
3238	248.14	249.08	FSU	2.4	48	5.9	1.48
3239	249.08	250.06	FSU	3.1	38.2	6.8	1.34
				Drill hole JOT_005			
4983	103.61	104.54	CSU	0.9	66.7	8.4	0.93
4984	104.54	105.56	CSU	1	83.8	7.4	1.30
4985	105.56	106.51	CSU	1.3	91.9	9.3	1.17
4986	106.51	107.49	CSU	1.3	94.5	9	1.24
4987	107.49	108.51	CSU	1.5	100	8.7	1.38
4988	108.51	109.12	CSU	1.6	89.8	8.1	1.39
4989	109.12	110.09	CSU	2.8	102	7.8	1.86
4990	110.09	111.04	CSU	4.1	104.8	8.2	2.08
4991	111.04	111.99	CSU	3.4	90.7	7.7	1.89
4992	111.99	112.94	CSU	2.5	98	8.9	1.53
4993	112.94	113.91	CSU	3.6	98.6	6.8	2.30
4994	113.91	114.86	CSU	3.7	96.6	8.3	1.88
4995	114.86	115.84	CSU	4.3	98.7	9.2	1.83
4996	115.84	116.82	CSU	4.2	92.4	8.8	1.83
4997	116.82	117.74	CSU	4.1	75.6	8.8	1.63
4998	117.74	118.69	CSU	4.5	94.6	7.5	2.25
4999	118.69	119.66	CSU	5.1	77.9	6.8	2.40
5001	119.66	120.74	CSU	5	81.1	8.7	1.89
5002	120.74	121.69	CSU	4.8	94.4	8.2	2.12
5003	121.69	122.65	CSU	3.2	90.8	8.6	1.65
5004	122.65	123.65	CSU	3.3	92	8.8	1.64
5005	123.65	124.59	CSU	3.1	89.7	7.7	1.81
5006	124.59	125.57	CSU	3.3	93.4	7.9	1.85
5007	125.57	126.55	CSU	3.3	96.4	7.6	1.96
5008	126.55	127.52	CSU	2.1	53	5.8	1.50
5009	127.52	128.5	CSU	3.4	107.5	7.6	2.12
5010	128.5	129.48	CSU	3.1	84.2	7.1	1.89
5011	129.48	130.38	CSU	3.2	98.5	8.2	1.82
5012	130.38	131.34	CSU	3.3	100.1	8.7	1.75
5013	131.34	132.32	CSU	3.3	90.9	7.9	1.82
5014	132.32	133.26	CSU	3.7	114.3	8.2	2.11
5015	133.26	134.24	CSU	3.4	98.5	7.8	1.96

Sample	From	To	Unit	Cs (ppm)	Rb (ppm)	Th (ppm)	((Cs + Rb)/Th) UCC
5016	134.24	134.76	CSU	3.8	106.5	8.1	2.06
5018	135.11	136.05	CSU	3.1	87	6.9	1.98
5019	136.05	137.09	CSU	3.3	96.8	8.2	1.82
5020	137.09	138.12	CSU	3.1	89.9	8.2	1.70
5022	138.12	139.07	CSU	3.5	91.6	8.7	1.70
5023	139.07	139.45	CSU	4.7	92.4	8	2.12
5024	139.45	140.12	CSU	6.2	109.6	8.9	2.39
5025	140.12	141.16	CSU	7.7	86.2	8.5	2.56
5026	141.16	142.12	CSU	7.1	87.2	8.1	2.56
5027	142.12	143.08	CSU	6.3	79.6	6.7	2.78
5028	143.08	143.75	CSU	7.3	90.6	7.1	3.02
5029	143.75	144.73	CSU	4.1	81.7	7.6	1.96
5030	144.73	145.68	CSU	5	82.5	8.2	2.02
5031	145.68	146.67	CSU	3.8	102.9	7.6	2.16
5032	146.67	147.66	CSU	3.2	79	6.2	2.11
5033	147.66	148.62	CSU	3.6	80.3	7	1.99
5034	148.62	149.6	CSU	3.3	91.4	7.7	1.87
5035	149.6	150.53	CSU	3	91.4	8	1.74
5036	150.53	151.47	CSU	3.4	99.4	8.8	1.74
5037	151.47	151.98	CSU	5.2	102.4	7.5	2.51
5038	151.98	152.94	CSU	6.8	106.6	7.9	2.79
5039	152.94	153.9	CSU	5.2	99.6	7.6	2.44
5040	153.9	154.93	CSU	4.1	100.2	8.5	1.96
5041	154.93	156.02	CSU	6.2	99.9	8.2	2.48
5043	156.02	157	CSU	6.9	100.7	7.9	2.74
5044	157	157.95	CSU	7.7	87.5	9.5	2.30
5045	157.95	158.93	CSU	6.4	81.4	8.2	2.32
5046	158.93	159.86	CSU	9.8	103.9	6.9	3.93
5047	159.86	160.8	CSU	7.7	96.5	8.6	2.64
5048	160.8	161.75	CSU	3	95.5	8.1	1.76
5049	161.75	162.8	CSU	2.6	95.2	7.5	1.80
5050	162.8	163.73	CSU	5	102.3	8.7	2.12
5051	163.73	164.68	CSU	6.6	108.2	8.5	2.57
5052	164.68	165.53	CSU	6.8	117.7	8.9	2.60
5053	165.53	166.61	CSU	2.7	83.4	7.1	1.78
5054	166.61	167.5	CSU	5.6	102	7.4	2.63
5055	167.5	168.47	CSU	4.2	91.1	8.5	1.88
5056	168.47	169.42	CSU	4.1	92.8	7.8	2.05
5057	169.42	170.32	CSU	5.6	105.9	8	2.48
5058	170.32	171.27	CSU	4.6	99	8.2	2.13
5059	171.27	172.25	CSU	4.8	90.6	7.8	2.18
5060	172.25	173.19	CSU	3.3	94.4	8.5	1.73
5061	173.19	174.16	CSU	3	83.7	7.9	1.67
5062	174.16	175.13	CSU	3.5	85.4	7.2	1.97
5064	175.13	176.06	CSU	4.4	91.1	9.4	1.74

Sample	From	To	Unit	Cs (ppm)	Rb (ppm)	Th (ppm)	((Cs + Rb)/Th) UCC
5065	176.06	177.05	CSU	6.2	106.1	8.3	2.52
5066	177.05	178.01	CSU	5.1	102.5	8.2	2.27
5067	178.01	178.93	CSU	4.4	99.5	7.7	2.22
5068	178.93	179.91	CSU	4.2	94.3	8.1	2.01
5069	179.91	180.93	CSU	4.6	77.3	5.6	2.75
5070	180.93	181.83	CSU	7.4	115.1	6.9	3.47
5071	181.83	182.8	CSU	8.2	118	6.1	4.20
5072	182.8	183.76	CSU	6.4	107.7	7	3.06
5073	183.76	184.74	CSU	7.4	105	7.7	2.98
5075	184.74	185.62	CSU	4.7	90.6	7.4	2.27
5076	185.62	186.58	CSU	5.7	92.2	7.5	2.50
5077	186.58	187.56	CSU	5.3	106.2	6.8	2.85
5078	187.56	188.47	CSU	4.4	105.6	6.1	2.90
5079	188.47	189.63	CSU	5	111.5	7.6	2.54
5080	189.63	190.76	CSU	5.8	96	8	2.41
5081	190.76	191.77	CSU	3.8	93	7.2	2.15
5082	191.77	192.75	BCSU	6.3	110.8	7.8	0.96
5083	192.75	193.71	BCSU	5.7	101.8	6.8	1.05
5084	193.71	194.25	BCSU	6	91.3	8.4	1.15
5086	194.25	195.01	BCSU	5	85.5	10.4	1.20
5087	195.01	195.86	BCSU	4.6	98.1	8.7	1.22
5088	195.86	197.11	BCSU	4.7	83.5	9.7	1.24
5089	197.11	197.98	BCSU	2.1	73.8	8.7	1.29
5090	197.98	198.96	BCSU	5	72	1.4	1.30
5091	198.96	199.9	BCSU	3.7	72.7	5.5	1.32
5092	199.9	200.84	BCSU	1.9	41.2	1.1	1.36
5093	200.84	201.81	BCSU	5.5	76.7	1.1	1.41
5094	201.81	202.78	BCSU	5.3	72.7	2.3	1.62
5095	202.78	203.52	BCSU	3.6	73.9	2.5	1.73
5096	203.52	204.49	BCSU	3.7	91.7	2.2	1.73
5097	204.49	205.47	BCSU	2.5	86.9	2.2	1.85
5098	205.47	206.35	BCSU	1.6	79.9	3	2.10
5099	206.35	207.36	BCSU	1.5	58.4	3.4	2.37
5100	207.36	208.29	BCSU	3.9	77.4	3.9	2.76
5101	208.29	209.29	BCSU	4.4	89.1	5.3	2.89
5102	209.29	209.8	BCSU	4.6	97.9	6.1	2.29
5104	210.22	211.21	BCSU	2.9	60	5.2	1.99
5106	211.21	212.16	FSU	1.8	65.1	4.2	1.67
5108	212.16	213.1	FSU	2.5	68.7	4.5	1.22
5109	213.1	214.05	FSU	2.4	59.1	3.2	11.16
5110	214.05	214.8	FSU	1.5	47	2.3	2.43
5111	214.8	215.56	BCSU	2.1	51.3	3.2	6.57
5112	215.56	216.4	BCSU	2.1	54.9	4	15.41
5113	216.4	217.48	BCSU	2.1	51.3	3.6	7.05
5114	217.48	218.44	BCSU	2	43.9	3.1	5.33

Sample	From	To	Unit	Cs (ppm)	Rb (ppm)	Th (ppm)	((Cs + Rb)/Th) UCC
5115	218.44	218.92	BCSU	2.5	57.7	2.2	6.89
5116	218.92	219.52	BCSU	2.9	58.3	3.7	5.72
5117	219.52	220.54	BCSU	1.7	30.3	1.5	3.44
5118	220.54	221.58	BCSU	2.8	60.5	6.1	2.39
5119	221.58	222.69	FSU	1.6	38.5	4.8	3.63
5120	222.69	223.12	FSU	0.6	16.5	2.4	3.05
5122	223.12	224.46	FSU	2.9	48.9	4.9	2.84
5123	224.46	224.73	BCSU	0.6	9.8	1.7	2.07
5124	224.73	225.73	FSU	2.6	63.2	6.4	2.67
5125	225.73	226.72	FSU	2.1	42.1	4.4	2.22
5142	240.74	241.69	FSU	1.7	35	2.6	0.34
5143	241.69	242.44	FSU	2.4	59.1	4.9	1.98
5144	242.44	243.4	FSU	0.7	30.8	7.6	1.12
5145	243.4	244.36	FSU	1.1	51.3	6.2	2.02
5146	244.36	245.29	FSU	0.6	42	6.5	1.68
5147	245.29	246.21	FSU	1.1	45.8	6.3	2.28
5148	246.21	247.17	BCSU	1.2	33.8	3	6.85
5149	247.17	248.16	BCSU	1.7	47.3	2.8	2.03
5151	248.16	249.13	BCSU	2	62.8	2.7	1.17
5152	249.13	250.08	BCSU	3.2	91.6	2.5	45.19
5153	250.08	251.06	BCSU	2.7	86.1	4	14.01
5154	251.06	252.02	BCSU	2.8	81.1	2.8	6.30
5155	252.02	253.07	BCSU	1.5	39.5	2.1	5.58
5156	253.07	254.1	BCSU	1.3	39	2.8	0.56
5157	254.1	255.02	BCSU	1	29.3	0.1	1.35
5158	255.02	256.01	BCSU	1.3	35.2	0.4	0.56
5159	256.01	257	BCSU	0.9	23.3	0.6	1.79
5160	257	257.97	BCSU	0.7	16.5	0.5	1.58
5161	257.97	259.39	BCSU	0.1	0.5	0.4	5.73
5162	259.39	260.35	BCSU	0.2	7.7	0.8	3.71
5163	260.35	261.3	BCSU	0.1	4.1	1	1.00
5164	261.3	262.28	BCSU	0.2	11.5	0.8	4.19
5165	262.28	263.23	BCSU	0.3	14.6	1.2	5.56
5166	263.23	263.71	BCSU	0.8	27.7	0.7	11.66
5167	263.71	264.83	BCSU	0.7	18.4	0.8	15.47
5168	264.83	265.96	BCSU	0.8	40.2	5.2	9.05
5169	265.96	267.08	BCSU	1.3	64.3	7.7	18.67
5170	267.08	268.03	BCSU	0.1	1.4	0.9	42.66
5172	268.03	269	BCSU	0.4	11.4	0.9	14.22
5173	269	269.94	BCSU	0.2	4.6	0.7	2.34
5174	269.94	270.9	BCSU	0.2	7	0.5	2.24
5175	270.9	271.77	BCSU	0.3	12.2	0.4	0.47
5176	271.77	272.66	BCSU	0.5	20.2	0.5	1.50
5177	272.66	273.6	BCSU	0.5	10.2	1.1	10.57
5178	273.6	274.59	BCSU	1.1	20.5	1.7	1.78

Sample	From	To	Unit	Cs (ppm)	Rb (ppm)	Th (ppm)	((Cs + Rb)/Th) UCC
5179	274.59	275.98	BCSU	0.9	20.3	0.3	4.14
5180	275.98	276.45	BCSU	1.3	24.9	0.3	7.84
5181	276.45	277.41	BCSU	1	19.7	0.4	5.27
5182	277.41	278.41	BCSU	0.9	22.8	0.2	20.12
5183	278.41	279.34	BCSU	1.1	24.7	0.1	3.37
5184	279.34	280.28	BCSU	0.4	7.6	0.1	1.12
5185	280.28	281.23	BCSU	0.1	0.6	0.1	2.62
5186	281.23	282.05	BCSU	0.1	0.5	0.1	1.31
5187	282.05	282.98	BCSU	0.1	2.1	0.8	2.24
5188	282.98	283.94	BCSU	0.1	1.3	0.2	2.24
5189	283.94	285.05	BCSU	0.9	16.8	0.3	2.60
5191	285.47	286.03	BCSU	0.2	3.8	0.4	2.24
5193	286.03	287.01	BCSU	0.8	21.4	0.5	0.22
5194	287.01	288.1	BCSU	1.3	31.6	2.6	2.37
5195	288.1	289.04	BCSU	0.4	10.1	0.4	11.76
5196	289.04	290	BCSU	1	22.9	0.5	2.48
5197	290	290.92	BCSU	1.9	42.7	1.4	1.66
5198	290.92	292	BCSU	0.5	12	0.1	11.45
5199	292	292.96	BCSU	0.1	1.7	0.1	3.85
5200	292.96	293.99	BCSU	0.1	2.9	0.4	4.21
5201	293.99	294.84	BCSU	0.1	0.9	0.1	14.41
5202	294.84	295.79	BCSU	0.1	0.9	0.2	13.19
5203	295.79	296.76	BCSU	0.1	0.5	0.1	11.85
5204	296.76	297.62	BCSU	0.1	0.5	0.1	15.60
5205	297.62	297.99	BCSU	0.3	5.4	0.4	12.85
5207	299.05	300.03	BCSU	0.1	0.5	0.1	2.42
5208	300.03	301.24	BCSU	0.1	0.9	1.2	3.06
5209	301.24	302.23	BCSU	0.8	20.2	1.4	3.07
5210	302.23	303.21	BCSU	0.9	20.6	0.3	1.34
5211	303.21	304.09	BCSU	0.1	3.4	0.2	1.09
5212	304.09	305.05	BCSU	0.2	3.3	0.4	1.99
5214	305.05	306	BCSU	0.8	21.5	0.3	1.65
5215	306	306.97	BCSU	0.5	11.1	0.5	1.74
5216	306.97	307.91	BCSU	0.1	2.6	0.1	2.42
5217	307.91	308.84	BCSU	0.4	7.8	0.1	2.00
5218	308.84	309.79	BCSU	0.7	14.9	0.2	0.54
5219	309.79	310.75	BCSU	0.9	20.9	0.3	1.09
5220	310.75	311.7	BCSU	1.6	36.3	0.4	0.77
5221	311.7	312.88	BCSU	1	22.2	0.3	0.99